THE UNIVERSITY OF SYDNEY

AEROSPACE ENGINERING
MASTER OF PHILOSOPHY

GALACTIC COLONISATION: GENERAL RELATIVISTIC INTERSTELLAR TRAJECTORY OPTIMISATION

Author:
Kenneth FUNG
SID: 309260221

Supervisors:
Dr. Xiaofeng WU
Prof. Geraint LEWIS

A thesis submitted in fulfilment of requirements for the degree of Master of Philosophy at the University of Sydney.

14th November 2016

Statement of Originality

I certify that the intellectual content of this thesis is the product of my own work and that all the assistance received in preparing this thesis and sources have been acknowledged.

Signed: . . . .   Student: Kenneth Fung

Date: 14th November 2016

Abstract

A vast wealth of literature exists on the topic of rocket trajectory optimisation, particularly in the area of interplanetary trajectories due to its relevance today. However, a large proportion of the research is focused on using a specific propulsion system, and is almost exclusively conducted using Newtonian mechanics. Studies on optimising interstellar and intergalactic trajectories are usually performed in flat spacetime using an analytical approach, with very little focus on optimising interstellar trajectories in a general relativistic framework.

This thesis examines the use of low-acceleration rockets to reach galactic destinations in the least possible time, with a genetic algorithm being employed for the optimisation process. The fuel required for each journey was calculated for various types of propulsion systems to determine the viability of low-acceleration rockets to colonise the Milky Way.

To limit the amount of fuel carried on board, it was found that an antimatter propulsion system would likely be the minimum technological requirement to reach star systems tens of thousands of light years away. However, using a low-acceleration rocket would require several hundreds of thousands of years to reach these star systems, with minimal time dilation effects since maximum velocities only reached about $0.2c$. Such transit times are clearly impractical, and it was concluded that low-acceleration rockets are not a viable candidate for galactic colonisation. High accelerations, on the order of $1\,\mathrm{g}$, are likely required to complete interstellar journeys within a reasonable time frame. To minimise fuel consumption, the propulsion system would likely need to be more advanced than an antimatter drive, though such a claim would require further research.

Preface

This thesis topic is a fusion between the realms of engineering and physics, and utilises tools from both fields to solve a complex problem in space travel.

This thesis focuses on the optimisation of interstellar trajectories using a general relativistic framework, an area which is becoming increasingly relevant as our technological ability advances and the human race continues to push into the cosmos.

As this is a rather unorthodox subject matter, extensive background material in both optimisation and relativity needs to be provided. All the underlying physics is derived and the engineering optimisation algorithm is explained in significant detail, so that one may hopefully follow on from the results of this research.

Acknowledgements

This thesis has been a strange journey, and its completion would not have been possible without the help of several individuals.

Firstly, I would like to thank my physics supervisor Prof. Geraint Lewis, who has continued to guide me even after completing my undergraduate honours thesis, and was very supportive of my chosen research topic.

I would also like to thank my engineering supervisor Dr. Xiaofeng Wu, who has been mentoring me since my second year of university. I would not be where I am now without his advice.

Finally, I am indebted to my friends and family for their continual support throughout my life. Their encouragements have kept me persevering during a tumultuous year. Wherever life takes me in the future, I will always be reminded that I would not be there without them.

And God said, "

$$\oint \mathbf{E} \cdot d\mathbf{A} = \frac{q}{\epsilon_0}$$

$$\oint \mathbf{B} \cdot d\mathbf{A} = 0$$

$$\oint \mathbf{E} \cdot d\mathbf{l} = -\frac{d}{dt} \int \mathbf{B} \cdot d\mathbf{A}$$

$$\oint \mathbf{B} \cdot d\mathbf{l} = \mu_0 \int \mathbf{J} \cdot d\mathbf{A} + \mu_0 \epsilon_0 \frac{d}{dt} \int \mathbf{E} \cdot d\mathbf{A}$$

," and there was light.

Contents

List of Figures

Chapter 1

Introduction

This chapter introduces the thesis topic, *Galactic Colonisation: General Relativistic Interstellar Trajectory Optimisation.* The objectives of the thesis will be addressed, and the motivations behind choosing this topic will be discussed to provide some context.

1.1 Objectives

Problem statement: *How should we vary the thrust and orientation of a low-acceleration rocket such that a traveller reaches a galactic destination in the least possible time? Knowing this, how viable is galactic colonisation using low-acceleration rockets?*

The aim of this research is to develop a genetic algorithm that can determine the rocket trajectory that reaches a destination within the Milky Way galaxy in the least possible time using a low-acceleration rocket. This in turn will determine the viability of low-acceleration rockets in colonising the Milky Way galaxy.

To approach this problem, it is first necessary to have a basic understanding of time dilation in general relativity. The thesis then focuses on deriving the equations of motion in curved spacetime and solving the resulting equations in Matlab. The theory behind genetic algorithms is presented, and a genetic algorithm is designed and implemented to optimise for the time experienced on board a rocket. Finally, several interstellar trajectories are considered using a low-acceleration rocket to determine the possibility of galactic colonisation.

1.2 Motivation

A wealth of literature exists on optimising space trajectories, in particular interplanetary trajectories due to its current and near-future applications. A majority of the research focuses on optimising trajectories for a specific propulsion system, rather than for a gen-

eral propulsion system that utilises the rocket equation. Solar sails appear to be the favourite propulsion candidate for trajectory optimisation due to the fact that there is no fuel consumption, hence considerably simplifying the analysis: Cassenti (1997) used basic calculus to optimise the solar system exit speed for a spacecraft using a solar sail; Zeng et al. (2011) optimised interplanetary solar sail trajectories with respect to the flight time using particle swarm optimisation; Dachwald (2004, 2005) used evolutionary neurocontrol to optimise low-thrust interplanetary trajectories; Kluever (1996) used sequential quadratic programming to optimise the flight time for a small spacecraft to reach the edge of the heliosphere[1] using solar and nuclear electric propulsion systems; and Abdelkhalik and Mortari (2007) used a genetic algorithm to optimise the fuel consumption during orbital transfers. However, solar sails are not practical for interstellar travel since they require a constant external source of energy, which is not always present in the expanse of interstellar space. Research conducted in optimising interstellar trajectories have mostly been performed within a Newtonian model, thereby simplifying the analysis by ignoring the relativistic effects of time dilation.

The discovery that time is relative has raised many interesting discussions, and has produced a plethora of literature on its effect on interstellar travel. Within the scientific community, many authors have examined the effects of time dilation whilst travelling interstellar and intergalactic distances, though all but a few of the calculations were performed in flat spacetime. Heyl (2005), Rindler (1960), and Kwan et al. (2010) considered the effect of an expanding universe when traversing intergalactic distances, and showed that a constant acceleration is necessary if one wishes to reach nearby galaxies within human lifetimes (though this is sensitive to the cosmological parameters used). In the currently favoured cosmological concordance model, a rocketeer accelerating at a constant rate of $g = 9.81\,\mathrm{m\,s^{-2}}$ is able to reach 99% of the way to the edge of the universe well within a human lifetime (Kwan et al., 2010), though upon return, many billions of years would have passed for those living on Earth.

Optimising an interstellar trajectory is an extremely complex and difficult task, and producing the correct solution may not always be possible. Almost all attempts consider either a Newtonian or special relativistic approach, as a general relativistic approach compounds the difficulty of the task. Henriques and Natario (2012) derived the optimality conditions for rocket trajectories in general relativity, though it was done from an analytical approach and did not consider any specific trajectories. To date, very little (if any) research has been performed on optimising interstellar trajectories in a general relativistic framework, and it is for this reason that this thesis topic was chosen. It is my hope that the results of this research will assist in the planning of future space missions when technology has advanced far enough for interstellar travel to be feasible.

---

[1]The *heliosphere* is the region of space that is dominated by the effects of the Sun, forming the boundary between our solar system and interstellar space.

Chapter 2

Relativity

This chapter provides the reader with an adequate understanding in relativity. Special relativity is first introduced, followed by general relativity, and concludes with a section introducing some required mathematics.

2.1 Special Relativity

Sir Isaac Newton's *Mathematical Principles of Natural Philosophy* set the foundations of scientific thought for the next three centuries. The *Principia*, as it is so called, contained Newton's formulation of classical mechanics (Newton, 1687), and remained unchallenged until Albert Einstein published his papers on special relativity in 1905.

2.1.1 Inconsistent Theories

The motivation of Einstein's special theory of relativity stems from the inconsistency between Newtonian mechanics and Maxwell's equations of electromagnetism.

Newtonian mechanics states that time is absolute and the addition of velocities is linear, which agrees with our intuition. Suppose we have two observers A and B, where A is stationary and B is in a moving car travelling past A at a relative speed v_1. If B throws a ball from the moving car at a speed v_2 (relative to B), then A will see the ball travel at speed of $v_1 + v_2$. Simple enough! We now replace the ball with a torch that emits a beam at the speed of light c. Relative to B, the light beam is travelling away from them at a speed c, whilst A sees the light beam travel away from them at a speed $v_1 + c$.

Maxwell's equations, as they are so often called, show that the speed of light (Griffiths, 1999) is

$$c = \frac{1}{\sqrt{\mu_0 \epsilon_0}} \approx 3 \times 10^8 \, \mathrm{m \, s^{-1}} \tag{2.1}$$

where μ_0 and ϵ_0 are the permeability and permittivity constants of free space respectively. Since there is no reference to the medium of propagation, it was widely believed that the speed of light predicted by Maxwell's equations was relative to some luminiferous aether. However, Einstein rejected this notion of an aether, and instead assumed that the speed of light was constant regardless of the motion of the observer. Consequently, Einstein believed that Newtonian mechanics would need to be modified since the linear addition of velocities would no longer be true.

2.1.2   The Fall of the Apple

Einstein assumed that Maxwell's equations were correct in all reference frames, implying that Newtonian mechanics needed to be modified. He made two simple assumptions that formed the groundwork for his theory:

- The principle of relativity: An inertial observer cannot experimentally determine whether they are stationary or moving at constant speed.
- The principle of invariant light speed: The speed of light in vacuum is constant in all reference frames.

From these simple assumptions, Einstein (1905) published a famous paper which marked the birth of relativity, titled *On the Electrodynamics of Moving Bodies*. The first postulate agrees with our intuitive understanding of the world; when you're a passenger in a car stuck in traffic and look out the window to the adjacent lane of cars that just begins moving, we sometimes feel as if we were the ones moving. The second postulate, however, required a completely radical notion of space and time.

Consider the following thought experiment, where an observer A on a moving train sees light rays bouncing perpendicularly between 2 mirrors spaced a distance L_0 apart. One mirror is on the roof and the other is on the floor, as shown in Fig. 2.1(a). Now consider another observer B stationary outside the train. If the train is moving in the $+x$ direction at a velocity v, then B will see the light rays trace the path shown in Fig. 2.1(b). Suppose both observers measure the time and distance taken for the light ray to bounce from the bottom to the top mirror. A will simply measure the distance to be L_0, taking a total time $\Delta t'$ of

$$\Delta t' = \frac{L_0}{c} \tag{2.2}$$

However, B will measure a slightly longer distance. If the time taken for the light ray to reach the roof is Δt, then B will measure the light ray to travel a total distance of $c\Delta t$. Since the train has now travelled forward by a distance of $v\Delta t$, then

$$(c\Delta t)^2 = L_0^2 + (v\Delta t)^2 \tag{2.3}$$

Substituting for L_0 from Equation (2.2) and rearranging gives
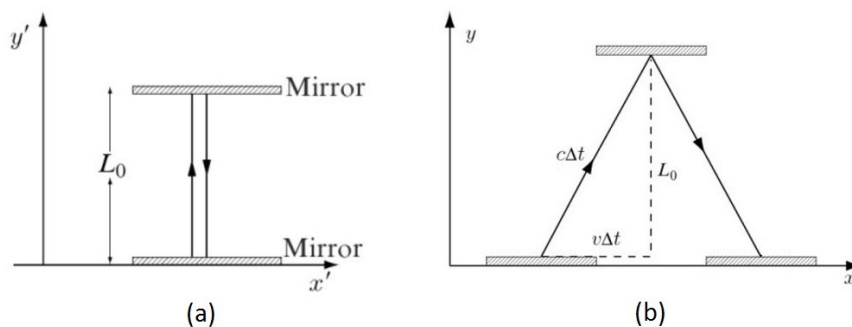
Figure 2.1: Relativity of simultaneity (Grøn and Hervik, 2007).

$$\Delta t' = \Delta t \sqrt{1 - \frac{v^2}{c^2}} = \frac{\Delta t}{\gamma} \qquad (2.4)$$

where

$$\gamma \equiv \left(1 - \frac{v^2}{c^2}\right)^{-1/2} \qquad (2.5)$$

is called the *Lorentz factor*. At $v = 0.5c$, $\gamma = 1.15$, and speeds above this are considered to be relativistic. Note that $\Delta t \geq \Delta t'$, that is, moving clocks run more slowly, a relativistic phenomenon known as *kinematic time dilation*. It must be remembered that time dilation is a direct result of the constancy of the speed of light. If the speed of light were not constant but instead depended on the velocity of the observer, then the above analysis would lead back to the Newtonian assumption of absolute time: $\Delta t' = \Delta t$.

If time is velocity-dependent, then space must also depend on velocity since $\Delta x = c\Delta t$. It is quite straightforward to show that

$$\Delta x' = \frac{\Delta x}{\gamma} \qquad (2.6)$$

This dilation of space is the relativistic phenomenon of known *length contraction*, and only occurs in the direction of motion. Again, if the speed of light were not constant but instead depended on the velocity of the observer, then the above analysis would lead back to the Newtonian result: $\Delta x' = \Delta x$.

In Newtonian mechanics, the time and space coordinates between two inertial frames moving with relative velocity v in the $+x$ direction are linked via the Galilean transformation:

$$t' = t \qquad (2.7)$$

$$x' = x - vt \qquad (2.8)$$

$$y' = y \qquad (2.9)$$

$$z' = z \qquad (2.10)$$

It can be shown (Hartle, 2003) that the equivalent relativistic transformations between two inertial frames are given by

$$t' = \gamma \left(t - \frac{vx}{c^2} \right) \tag{2.11}$$

$$x' = \gamma(x - vt) \tag{2.12}$$

$$y' = y \tag{2.13}$$

$$z' = z \tag{2.14}$$

These equations are known as the *Lorentz transformation*. As expected, the Lorentz transformation reduces to the Galilean transformation when $v \ll c$.

2.1.3   Spacetime

The constancy of the speed of light inevitably means that space and time are linked, and hence can be unified into one coordinate system (t, x, y, z), known as *spacetime*. The term *flat* spacetime is used to describe the geometry of special relativity.

The mathematical description of any geometric surface can be described by a line element (or interval), which calculates the infinitesimal distance ds between two points on the surface on the geometry. In Euclidean geometry, the line element is given by

$$ds^2 = dx^2 + dy^2 + dz^2 \tag{2.15}$$

Equivalently, polar coordinates, or any other coordinate system could be used to calculate the distance between two points in Euclidean space, and the measured distance is independent of the coordinate system used. In mathematical terms, this line element is *invariant* under a coordinate transformation.

In special relativity, time and space are interlinked. Consequently, the distance between two points will also depend on the time coordinate. In a similar manner to Euclidean space, the line element in flat spacetime must remain invariant under a change in inertial frames, that is, under a Lorentz transformation. As it turns out, the interval

$$ds^2 = -c^2 dt^2 + dx^2 + dy^2 + dz^2 \tag{2.16}$$

remains invariant under a Lorentz transformation (Feynman et al., 2011). Equation (2.16) is known as the *Minkowski metric*, and is the line element of flat spacetime.

The *proper time* τ is defined as the time measured by a clock travelling with an observer. For a stationary observer, $dt = d\tau$ and $dx = dy = dz = 0$, and Equation (2.16) reduces to $ds^2 = -c^2 d\tau^2$. Hence, the proper time is related to the line element through

$$d\tau^2 = -\frac{ds^2}{c^2} \tag{2.17}$$

2.2 General Relativity

The flat spacetime of special relativity is derived from the assumption that it is sufficiently far from any gravitational sources. Just as Newtonian mechanics is the low-speed approximation of special relativity, special relativity is the low-mass approximation of a more general theory: general relativity.

2.2.1 The Equivalence Principle

The *equivalence principle* was one of the guiding principles of general relativity (Einstein, 1907), and states the equality between gravitation and acceleration. Consider the following scenario, Fig. 2.2(a), where an observer A is inside an elevator accelerating upwards at a rate of $g = 9.81 \, \mathrm{m \, s^{-2}}$, far from any gravitational influence, and an observer B is stationary on earth. If both observers drop a ball, each will measure the ball falling at a rate of g, and neither of them can distinguish which scenario they are in. Therefore, in a similar manner to the principle of relativity, the equivalence principle asserts that an observer cannot experimentally distinguish between a uniform acceleration and a uniform gravitational field.
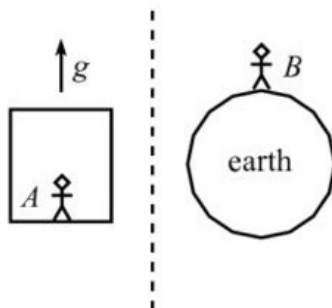
Figure 2.2: The Equivalence Principle (Morin, 2008).

2.2.2 Gravitational time dilation

We now apply the equivalence principle to deduce another source of time dilation. Consider the following scenario, where the space shuttle is accelerating at a uniform rate to the right, Fig. 2.3. Two observers (or astronauts), A and B, are placed at either end of the shuttle. Observer A is at the fore of the shuttle holding a transmitter, whilst observer B is at the aft holding a receiver. Now suppose observer A transmits signals at equally spaced time intervals. As the rocket is accelerating to the right, observer B will receive the signals at an increased frequency due to the constancy of the speed of light, and is in fact experiencing shorter time intervals than observer A. The equivalence principle then implies that clocks run slower in a lower gravitational potential, a general relativistic effect known as *gravitational time dilation* (Einstein, 1915).

Figure 2.3: Gravitational time dilation (Cheng, 2015).

2.3   Mathematics of Relativity

The flat spacetime of special relativity was applicable assuming zero gravitational influence. In reality, there are massive bodies around us that exert a gravitational field that cannot be ignored. Einstein predicted that massive bodies curved the surrounding four-dimensional spacetime geometry, producing the phenomena we know as gravity, Fig. 2.4. To describe the mathematics of curved spacetime, some mathematical concepts will first need to be introduced.
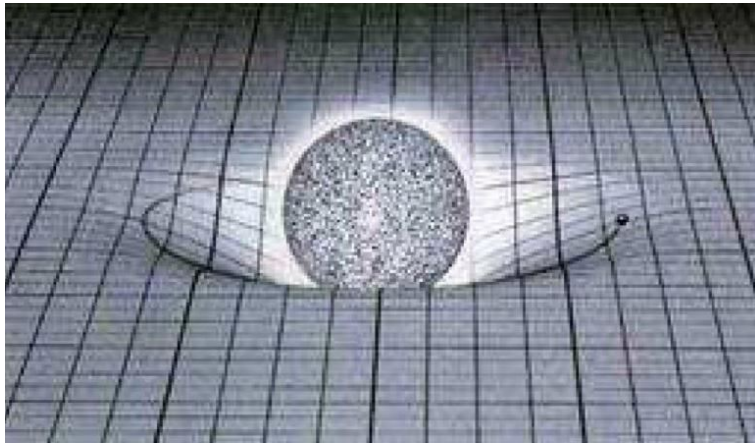
Figure 2.4: An object orbiting a massive body in curved spacetime (Glendenning, 2007).

2.3.1   Four-vectors

In Euclidean geometry, vectors have three components to describe their magnitude and orientation. The *four-vector* is the relativistic analogue of the Euclidean three-vector. For example, the displacement four-vector $\mathbf{x}$ is the coordinates of a point (t, x, y, z) in space-time. Four-vectors are similar to the Euclidean three-vector in that they obey the usual addition and multiplication rules, but are different in that four-vectors remain invariant under a Lorentz transformation. The magnitude of a four-vector is equal to the length of the vector as determined by the line element of the local spacetime geometry.

In a particular inertial frame, a four-vector can be decomposed along a set of four

orthogonal basis vectors, $\mathbf{e}_0, \mathbf{e}_1, \mathbf{e}_2, \mathbf{e}_3$, so that any four-vector $\mathbf{a}$ can be expressed as

$$\mathbf{a} = a^0\mathbf{e}_0 + a^1\mathbf{e}_1 + a^2\mathbf{e}_2 + a^3\mathbf{e}_3 = \sum_{\alpha=0}^{3} a^\alpha \mathbf{e}_\alpha = a^\alpha \mathbf{e}_\alpha \tag{2.18}$$

where the last equality was written using Einstein summation convention, in which repeated indices are understood to be summed over.

In Euclidean geometry, the scalar product of two three-vectors $\mathbf{a}$ and $\mathbf{b}$ is given by

$$\mathbf{a} \cdot \mathbf{b} = a^x b^x + a^y b^y + a^z b^z = a^\alpha b^\alpha \tag{2.19}$$

In curved spacetime, the scalar product of two four-vectors $\mathbf{a}$ and $\mathbf{b}$ is given by

$$\mathbf{a} \cdot \mathbf{b} = g_{\alpha\beta} a^\alpha b^\beta \tag{2.20}$$

where

$$g_{\alpha\beta} = \mathbf{e}_\alpha \cdot \mathbf{e}_\beta \tag{2.21}$$

is the *metric* of the spacetime geometry (Hartle, 2003), related to the line element via

$$ds^2 = d\mathbf{x} \cdot d\mathbf{x} = g_{\alpha\beta} dx^\alpha dx^\beta \tag{2.22}$$

For flat spacetime,

$$-c^2 dt^2 + dx^2 + dy^2 + dz^2 = \eta_{\alpha\beta} dx^\alpha dx^\beta \tag{2.23}$$

and we see that the metric of flat spacetime, $\eta_{\alpha\beta}$, is given by

$$\eta_{\alpha\beta} = \mathrm{diag}(-c^2, 1, 1, 1) \tag{2.24}$$

For curved spacetime, the metrics will depend on the physics of the surroundings.

2.3.2   Normalisation Conditions

The distance travelled in spacetime depends on the line element, and is therefore a function of the proper time. Thus, four-vectors can be parameterised in terms of the proper time τ, so that $x^\alpha = x^\alpha(\tau)$. Differentiating this leads to the *four-velocity u^α*,

$$u^\alpha = \frac{dx^\alpha}{d\tau} \tag{2.25}$$

which can be further differentiated to give the *four-acceleration* a^α,

$$a^\alpha = \frac{d^2 x^\alpha}{d\tau^2} \tag{2.26}$$

The following normalisation condition for $\mathbf{u}$ is then obtained:

$$\mathbf{u} \cdot \mathbf{u} = g_{\alpha\beta} \frac{dx^\alpha}{d\tau} \frac{dx^\beta}{d\tau} = \left(\frac{ds}{d\tau}\right)^2 = -c^2 \tag{2.27}$$

This implies that

$$\frac{d}{d\tau}(\mathbf{u} \cdot \mathbf{u}) = 0 \tag{2.28}$$

$$\Rightarrow \mathbf{u} \cdot \mathbf{a} = 0 \tag{2.29}$$

2.3.3   Geodesics

In curved spacetime, a test particle without any external forces acting on it will follow a trajectory that depends on the surrounding spacetime curvature. This path, known as a *geodesic*, expands upon the Euclidean notion of a straight line to curved spacetime. In curved spacetime, a geodesic is the shortest path between two points, just like how a straight line is the shortest path between two points in Euclidean geometry.

To determine the equations of motion, a calculus of variations approach can be employed to determine the shortest distance. The action S to be minimised is

$$S = \int ds = \int \sqrt{-g_{\alpha\beta} \frac{dx^\alpha}{d\tau} \frac{dx^\beta}{d\tau}} \, d\tau = \int \mathcal{L} \, d\tau \tag{2.30}$$

where $\mathcal{L}$ is the functional (or Lagrangian). Setting $\delta S = 0$ leads to the Euler-Lagrange equations:

$$\frac{d}{d\tau}\left(\frac{\partial \mathcal{L}}{\partial \dot{x}^\alpha}\right) = \frac{\partial \mathcal{L}}{\partial x^\alpha} \tag{2.31}$$

These equations are then solved (Hartle, 2003), leading to the *geodesic equation*

$$\frac{d^2 x^\alpha}{d\tau^2} = -\Gamma^\alpha_{\beta\gamma} \frac{dx^\beta}{d\tau} \frac{dx^\gamma}{d\tau} \tag{2.32}$$

where

$$g_{\alpha\delta} \Gamma^\delta_{\beta\gamma} = \frac{1}{2}\left(\frac{\partial g_{\alpha\beta}}{\partial x^\gamma} + \frac{\partial g_{\alpha\gamma}}{\partial x^\beta} - \frac{\partial g_{\beta\gamma}}{\partial x^\alpha}\right) \tag{2.33}$$

The Γ terms are known as the *Christoffel symbols* of the spacetime geometry. The Christoffel symbols for simple spacetime geometries are readily available in literature.

For the Minkowski metric (flat spacetime), the Christoffel symbols are all 0, and the

geodesic equation reduces to

$$\frac{d^2 x^\alpha}{d\tau^2} = 0 \tag{2.34}$$

Thus, a particle travelling at constant speed in flat spacetime will remain at a constant speed, in agreement with Newton's second law of motion.

For an accelerated observer with four-acceleration a^α, the equations of motion become (Stephani, 2004)

$$\frac{d^2 x^\alpha}{d\tau^2} = -\Gamma^\alpha_{\beta\gamma} \frac{dx^\beta}{d\tau} \frac{dx^\gamma}{d\tau} + a^\alpha \tag{2.35}$$

Note that Equations (2.32) and (2.35) consists of 4 coupled ordinary differential equations (ODE's), which need to be solved to determine the motion of an observer. Except for the most simplest of geometries, the equations of motion need to be solved computationally.

2.3.4   Three-velocity

To compute the three-velocity of a particle, we need to convert the four-velocities into a measurable three-velocity. Quantities that can be measured in the observer's frame of reference can be decomposed into four orthogonal unit four-vectors $\mathbf{e}_{\hat{\alpha}}$, forming an orthonormal basis (Hartle, 2003). As the observer is in a local inertial frame, then

$$\mathbf{e}_{\hat{\alpha}} \cdot \mathbf{e}_{\hat{\beta}} = \eta_{\hat{\alpha}\hat{\beta}} \tag{2.36}$$

In contrast, immeasurable (but calculated) quantities such as the four-velocity are expressed in a coordinate basis, where

$$\mathbf{e}_{\alpha} \cdot \mathbf{e}_{\beta} = g_{\alpha\beta} \tag{2.37}$$

The relationship between orthonormal and coordinate bases is given by

$$a^\alpha = a^{\hat{\beta}} (\mathbf{e}_{\hat{\beta}})^\alpha \tag{2.38}$$

$$a^{\hat{\beta}} = a^\alpha (\mathbf{e}_{\alpha})^{\hat{\beta}} \tag{2.39}$$

For a diagonal metric, the orthonormal and coordinate basis vectors are given by (Hartle, 2003)

$$
\begin{aligned}
(\mathbf{e}_{\hat{0}})^\alpha &= [(-g_{00})^{-1/2}, 0, 0, 0] & (\mathbf{e}_0)^{\hat{\alpha}} &= [(-g_{00})^{1/2}, 0, 0, 0] \\
(\mathbf{e}_{\hat{1}})^\alpha &= [0, g_{11}^{-1/2}, 0, 0] & (\mathbf{e}_1)^{\hat{\alpha}} &= [0, g_{11}^{1/2}, 0, 0] \\
(\mathbf{e}_{\hat{2}})^\alpha &= [0, 0, g_{22}^{-1/2}, 0] & (\mathbf{e}_2)^{\hat{\alpha}} &= [0, 0, g_{22}^{1/2}, 0] \\
(\mathbf{e}_{\hat{3}})^\alpha &= [0, 0, 0, g_{33}^{-1/2}] & (\mathbf{e}_3)^{\hat{\alpha}} &= [0, 0, 0, g_{33}^{1/2}]
\end{aligned}
\tag{2.40}
$$

Hence, the four-velocities can now be transformed to the orthonormal frame:

$$u^{\hat{t}} = u^t(\mathbf{e}_t)^{\hat{t}} + u^x(\mathbf{e}_x)^{\hat{t}} + u^y(\mathbf{e}_y)^{\hat{t}} + u^z(\mathbf{e}_z)^{\hat{t}} = u^t(-g_{tt})^{1/2} \tag{2.41}$$

$$u^{\hat{x}} = u^t(\mathbf{e}_t)^{\hat{x}} + u^x(\mathbf{e}_x)^{\hat{x}} + u^y(\mathbf{e}_y)^{\hat{x}} + u^z(\mathbf{e}_z)^{\hat{x}} = u^x g_{ii}^{1/2} \tag{2.42}$$

$$u^{\hat{y}} = u^t(\mathbf{e}_t)^{\hat{y}} + u^x(\mathbf{e}_x)^{\hat{y}} + u^y(\mathbf{e}_y)^{\hat{y}} + u^z(\mathbf{e}_z)^{\hat{y}} = u^y g_{ii}^{1/2} \tag{2.43}$$

$$u^{\hat{z}} = u^t(\mathbf{e}_t)^{\hat{z}} + u^x(\mathbf{e}_x)^{\hat{z}} + u^y(\mathbf{e}_y)^{\hat{z}} + u^z(\mathbf{e}_z)^{\hat{z}} = u^z g_{ii}^{1/2} \tag{2.44}$$

The three-velocity is therefore

$$v = \sqrt{\left(\frac{d\hat{x}}{d\hat{t}}\right)^2 + \left(\frac{d\hat{y}}{d\hat{t}}\right)^2 + \left(\frac{d\hat{z}}{d\hat{t}}\right)^2} \tag{2.45}$$

$$= \sqrt{\left(\frac{u^{\hat{x}}}{u^{\hat{t}}}\right)^2 + \left(\frac{u^{\hat{y}}}{u^{\hat{t}}}\right)^2 + \left(\frac{u^{\hat{z}}}{u^{\hat{t}}}\right)^2} \tag{2.46}$$

$$= \sqrt{-\frac{g_{ii}}{g_{tt}}\left(\frac{u^x}{u^t}\right)^2 - \frac{g_{ii}}{g_{tt}}\left(\frac{u^y}{u^t}\right)^2 - \frac{g_{ii}}{g_{tt}}\left(\frac{u^z}{u^t}\right)^2} \tag{2.47}$$

$$= \sqrt{-\frac{g_{ii}[(u^x)^2 + (u^y)^2 + (u^z)^2]}{g_{tt}(u^t)^2}} \tag{2.48}$$

$$= c\sqrt{\frac{c^2 + g_{tt}(u^t)^2}{g_{tt}(u^t)^2}} \tag{2.49}$$

$$\Rightarrow v = c\sqrt{1 + \frac{c^2}{g_{tt}(u^t)^2}} \tag{2.50}$$

Note that the velocity must always be less than the speed of light since $g_{tt} < 0$.

Chapter 3

Galactic Model

This chapter details the Milky Way mass model used for the trajectory calculations. The structure of the Milky Way is explored, followed by the equations of motion within the mass model.

3.1 Milky Way Mass Model

The Milky Way is a barred spiral galaxy that hosts our Sun along with more than hundreds of billions of other stars and planets, with a total visible mass on the order of $10^{11}\,\mathrm{M_\odot}$ (solar mass)[1]. The size and mass estimates of the Milky Way varies depending on the methodology used, and have some degree of uncertainty in them. One reason for this is due to the presence of exotic dark matter, of which we know very little about. Analysis of the galactic rotation curve of the Milky Way show that the orbital velocity is far too high for the amount of observable matter in the galaxy (Koupelis and Kuhn, 2007), and that a huge amount of invisible mass must be present in the form of a halo around the galaxy. This missing mass is attributed to dark matter, and is calculated to contribute at least 80-90% of the total mass of the Milky Way. As dark matter cannot be detected via light, it is understandably difficult to ascertain the exact size and mass of the Milky Way. However, there are commonly accepted values in literature which will be sufficient for this research task.

The structure of the Milky Way can be separated into three components: the central bulge, the galactic disk, and the dark matter halo. The central bulge is spheroidal in shape, stretching about $3\,\mathrm{kpc}$ across its longest diameter[2], and consists mainly of older stars. The galactic disk has a diameter of about $30\,\mathrm{kpc}$ with an average thickness of roughly $0.3\,\mathrm{kpc}$ (Rix and Bovy, 2013), and consists of five spiral arms. The edge of the dark matter halo is hard to define, but extends out to a radius of at least $100\,\mathrm{kpc}$ (Jones

---

[1]$1\,M_\odot \approx 1.99 \times 10^{30}\,\mathrm{kg}$
[2]$1\,\mathrm{pc} \approx 3.26$ ly

and Lambourne, 2004). Fig. 3.1 is a Matlab-generated plot of the Milky Way.
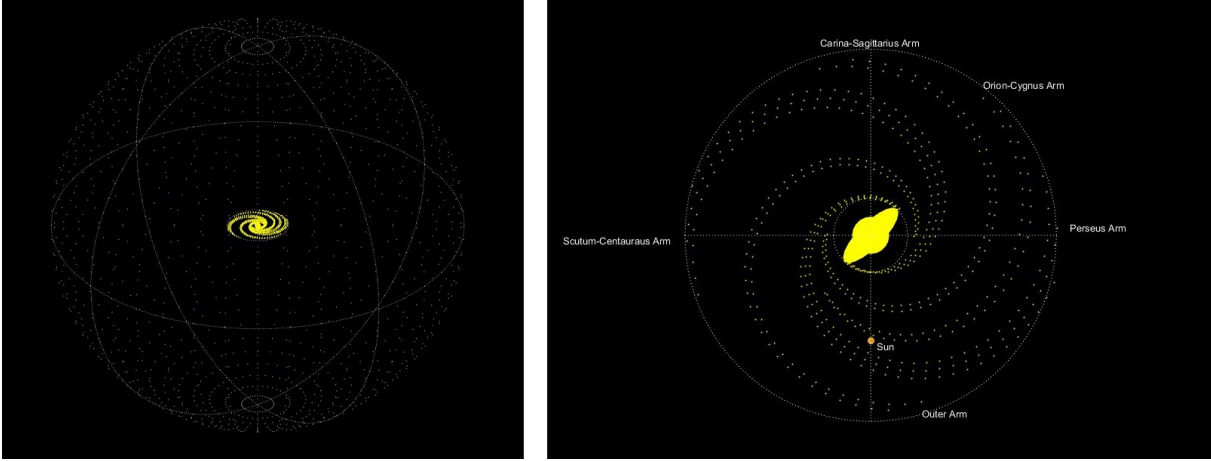
Figure 3.1: Structure of the Milky Way.

3.1.1   The Gravitational Model

To model the effect of spacetime curvature due to the mass of the Milky Way, the *static weak field metric* will be used, which describes the spacetime geometry in a weak, time-independent, gravitational field, such as that of the Milky Way (Gasperini, 2013). The static weak field depends on the Newtonian gravitational potential Φ, and is described by the metric

$$ds^2 = -\left(1 + \frac{2\Phi}{c^2}\right)(c\,dt)^2 + \left(1 - \frac{2\Phi}{c^2}\right)(dx^2 + dy^2 + dz^2) \tag{3.1}$$

The gravitational potential due to the Milky Way galaxy is made up from the gravitational effects of the bulge, disk, and halo. Various gravitational models exist for each of these components, and has varying degrees of success. The following gravitational models are some of the most successful and commonly used models in literature, and will be used here to model the Milky Way:

- Miyamoto-Nagai disk
- Hernquist bulge
- Navarro-Frenk-White (NFW) halo

The potential of the Miyamoto-Nagai disk (Miyamoto and Nagai, 1975) is given by

$$\Phi_d = -\frac{GM_d}{\sqrt{x^2 + y^2 + \left(r_d + \sqrt{z^2 + b_d^2}\right)^2}} \tag{3.2}$$

where G is the universal gravitational constant, M_d is the mass of the disk, r_d is the scale length of the disk, and b_d is the scale height of the disk.

The potential of the Hernquist Bulge (Hernquist, 1990) is given by

$$\Phi_b = -\frac{GM_b}{\sqrt{x^2 + y^2 + z^2} + r_b} \tag{3.3}$$

where M_b is the mass of the bulge and r_b is the scale length of the bulge.

The potential of the Navarro-Frenk-White Halo (Navarro et al., 1997) is given by

$$\Phi_h = -\frac{GM_h}{\sqrt{x^2 + y^2 + z^2}} \ln \left(\frac{\sqrt{x^2 + y^2 + z^2}}{r_h} + 1 \right) \tag{3.4}$$

where M_h is the mass of the halo and r_h is the scale length of the halo.

The gravitational potential of the Milky Way is then the sum of these components:

$$\Phi = \Phi_d + \Phi_b + \Phi_h \tag{3.5}$$

3.1.2   Galactic Parameters of the Milky Way

As mentioned before, there are only estimates of the mass and scale lengths of the Milky Way galaxy. However, over the years, researchers have narrowed down the range of possible values based on the latest observational data, scientific models, and numerical simulations.

For the Miyamoto-Nagai disk, the mass and scale lengths are (Nusser, 2009)

- $M_d = 10 \times 10^{10} \ M_\odot$
- $r_d = 6.5$ kpc
- $b_d = 0.26$ kpc

For the Hernquist bulge, the mass and scale lengths are (Koposov et al., 2010)

- $M_b = 3.4 \times 10^{10} \ M_\odot$
- $r_b = 0.7$ kpc

For the NFW potential, the mass and scale lengths are calculated from the *virial mass* M_v of the halo, which is the enclosed halo mass at the *virial radius* R_v. The exact size of a galaxy is difficult to quantify as the halo mass density extends out continuously into intergalactic space. The virial radius can be thought of as the radius beyond which the halo blends into the background matter in the universe. For the Milky Way, the virial mass is roughly (Dehnen et al., 2006)

- $M_v = 150 \times 10^{10} \ M_\odot$

The virial radius is calculated from the virial mass using (Kafle et al., 2014)

$$R_v = \left(\frac{2 M_v G}{H_0^2 \Omega_m \Delta_{th}} \right)^{1/3} \approx 294.5 \, \text{kpc} \tag{3.6}$$

where H_0 is the Hubble constant that describes the expansion of the universe, Ω_m is the matter density of the universe, and Δ_{th} is the over-density of dark matter compared to the average matter density. The latest cosmological parameters obtained from the 9 year mission of the Wilkinson Microwave Anisotropy Probe (WMAP) (Bennett et al., 2013) are

- $H_0 = 70.4 \times 10^{-3} \, \text{km} \, \text{s}^{-1} \, \text{Mpc}^{-1}$
- $\Omega_m = 0.3$
- $\Delta_{th} = 340$

The mass and scale lengths of the dark matter halo are related to the virial mass and virial radius via the dark matter halo concentration, which is described by the *halo concentration parameter* c_h, approximated by (Bullock and Johnston, 2005)

$$c_h \simeq 9.6 \left(\frac{M_v}{10^{13} M_\odot} \right)^{-0.13} (1 + z)^{-1} \approx 12 \tag{3.7}$$

where z is the redshift, which is zero for host dark matter halos. The mass (de Naray et al., 2009) and scale length (Kafle et al., 2012) of the halo are then given by

$$M_h = \frac{M_v}{\ln(c_h + 1) - \frac{c_h}{c_h + 1}} \approx 91.4 \times 10^{10} \, M_\odot \tag{3.8}$$

$$r_h = \frac{R_v}{c_h} \approx 24.5 \, \text{kpc} \tag{3.9}$$

Contour plots of the potentials in the galactic plane and perpendicular to the galactic plane are shown in Fig. 3.2, where the lines represent the size of the bulge, disk, and halo.

3.2   The Rocket Equation

The rocket equation describes the motion of a projectile that produces thrust by ejecting mass. By applying the Newtonian laws of conservation of momentum and mass, it can be shown that the Newtonian rocket equation is given by (Moore, 1813; Tsiolkovsky, 1903)

$$\Delta v = v_e \ln \frac{m_i}{m_f} \tag{3.10}$$

where Δv is the total change in velocity of the rocket, v_e is the effective exhaust velocity of the propellants, and m_i and m_f are the initial and final mass of the rocket, respectively.
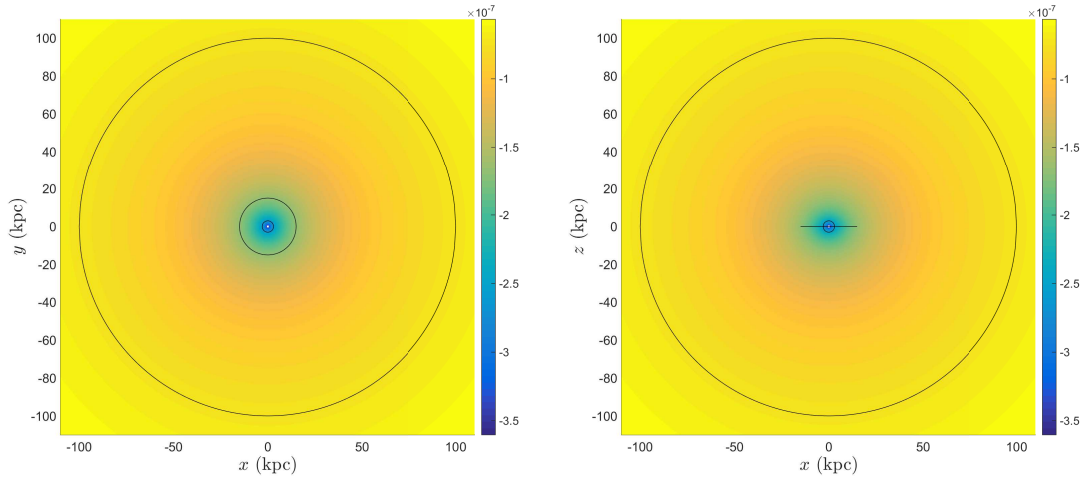
Figure 3.2: Gravitational potential of the Milky Way.

However, for relativistic speeds and exhaust velocities, a special relativistic derivation is required. The special relativistic result can then be applied to curved spacetime, since the equivalence principle implies that at every point in curved spacetime, there exists a local inertial frame where the local properties of curved spacetime are indistinguishable from the properties of flat spacetime (Hartle, 2003).

By applying the relativistic conservation of momentum and the conservation of mass-energy, Esnault-Pelterie and Lahure (1930) and Ackeret (1946) showed that the relativistic rocket equation is given by

$$\Delta v = c \tanh \left(\frac{v_e}{c} \ln \frac{m_i}{m_f} \right) \tag{3.11}$$

Bade (1953) showed that the proper acceleration a (i.e. the acceleration as experienced by the traveller) is related to the rate of change of mass of the rocket,

$$\frac{1}{c} \int_0^\tau a \, d\tau = -\frac{v_e}{c} \int_0^\tau \frac{1}{m} \frac{dm}{d\tau} \, d\tau \tag{3.12}$$

Therefore, the proper acceleration experienced on board the rocket is given by

$$a = -\frac{v_e}{m} \frac{dm}{d\tau}, \quad \frac{dm}{d\tau} \leq 0 \tag{3.13}$$

The mass of the rocket at any point along the trajectory can then be determined:

$$\frac{dm}{d\tau} = -\frac{ma}{v_e} \tag{3.14}$$

$$\Rightarrow \int_{m_i}^m \frac{dm}{m} = -\frac{1}{v_e} \int_0^\tau a \, d\tau \tag{3.15}$$

$$\Rightarrow m = m_i \exp \left(-\frac{1}{v_e} \int_0^\tau a \, d\tau \right) \tag{3.16}$$

The total required mass of the rocket m_0 on launch can then be calculated if the final mass and proper time are known. Assuming that the rocket expends all its fuel after a proper time of τ_f, then

$$m_0 = m_r \exp\left(\frac{1}{v_e}\int_0^{\tau_f} a(\tau)\, d\tau\right) \tag{3.17}$$

where m_r is the final mass, or equivalently, the mass of the rocket without fuel. If the mass of the fuel is m_f, then $m_0 = m_f + m_r$, and hence

$$m_f = m_r\left[\exp\left(\frac{1}{v_e}\int_0^{\tau_f} a(\tau)\, d\tau\right) - 1\right] = m_r\beta \tag{3.18}$$

where β is the fuel-to-empty rocket mass ratio. Smaller values of v_e will result in a larger value of β, and hence more fuel will be required as expected.

3.3 Equations of Motion

To compute the rocket trajectories around the Milky Way, we need to prescribe an acceleration four-vector for Equation (2.35). Given the magnitude of the proper acceleration, a, we determine the components of the four-acceleration by setting the thrust vector. We let the spatial components of the four-acceleration be

$$a^i = (a^x, a^y, a^z) = a_s(a_x, a_y, a_z) \tag{3.19}$$

where a_x, a_y, and a_z are the components of a unit vector, so that

$$a^i = a_s(a_x\hat{\mathbf{x}} + a_y\hat{\mathbf{y}} + a_z\hat{\mathbf{z}}) = |a^i|(a_x\hat{\mathbf{x}} + a_y\hat{\mathbf{y}} + a_z\hat{\mathbf{z}}) \tag{3.20}$$

and

$$a_x^2 + a_y^2 + a_z^2 = 1 \tag{3.21}$$

The values of a^t and a_s are determined via the normalisation conditions from Equations (2.27) and (2.29). Applying Equation (2.27) to the static weak field metric gives

$$g_{tt}(a^t)^2 + g_{ii}a_s^2 = a^2 \tag{3.22}$$

where the metric terms are

$$g_{tt} = -c^2\left(1 + \frac{2\Phi}{c^2}\right) \tag{3.23}$$

$$g_{ii} = 1 - \frac{2\Phi}{c^2} \tag{3.24}$$

Applying Equation (2.29) to the static weak field metric gives

$$g_{tt}u^t a^t + g_{ii}a_s k = 0 \tag{3.25}$$

where

$$k \equiv u^x a_x + u^y a_y + u^z a_z \tag{3.26}$$

Solving Equations (3.22) and (3.25) together, we get

$$a^t = \mp ak\frac{g_{ii}}{g_{tt}}\sqrt{\frac{g_{tt}}{g_{ii}[g_{ii}k^2 + g_{tt}(u^t)^2]}} \tag{3.27}$$

$$a_s = \pm au^t\sqrt{\frac{g_{tt}}{g_{ii}[g_{ii}k^2 + g_{tt}(u^t)^2]}} \tag{3.28}$$

where the positive sign for a_s is taken to produce the intended directions.

Thus, the acceleration four-vector can be input into the equations of motion if the thrust vector (a_x, a_y, a_z) is specified. The Christoffel symbols are calculated from Equation (2.33), where the potential in the metric terms is given by Equation (3.5).

3.4 The Matlab Solver

The equations of motion are integrated using Matlab's `ode45` solver, which is a non-stiff solver that utilises an explicit fifth-order Runge-Kutta method. The solver computes the solution to a set of first order ODE's given the initial conditions (IC's) over a specified period of integration. In this case, we have four second-order ODE's (the equations of motion) and one first order ODE (for the mass of the rocket, Equation (3.14)). The equations of motion can be rewritten as a set of 8 first-order ODE's:

$$\begin{aligned}
\frac{dt}{d\tau} &= u^t & \frac{du^t}{d\tau} &= -\Gamma^t_{\beta\gamma}u^\beta u^\gamma + a^t \\
\frac{dx}{d\tau} &= u^x & \frac{du^x}{d\tau} &= -\Gamma^x_{\beta\gamma}u^\beta u^\gamma + a_s a_x \\
\frac{dy}{d\tau} &= u^y & \frac{du^y}{d\tau} &= -\Gamma^y_{\beta\gamma}u^\beta u^\gamma + a_s a_y \\
\frac{dz}{d\tau} &= u^z & \frac{du^z}{d\tau} &= -\Gamma^z_{\beta\gamma}u^\beta u^\gamma + a_s a_z
\end{aligned} \tag{3.29}$$

The only unknown initial condition is the time component of the four-velocity, which can be found by rearrangement of Equation (2.27), giving

$$u^t = \pm\sqrt{-\frac{c^2 + g_{ii}[(u^x)^2 + (u^y)^2 + (u^z)^2]}{g_{tt}}} \tag{3.30}$$

where the positive sign is taken since $u^t \geq 1$.

Once the nine first-order ODE's are solved, the solution y is output as a set of column vectors parameterised in terms of τ,

$$y = \begin{bmatrix} t & x & y & z & u^t & u^x & u^y & u^z & m \end{bmatrix} \tag{3.31}$$

All the required variables can then be obtained from this solution. The accuracy of the solution is determined by checking that the normalisation conditions in Equation (2.27) and (2.29) hold for each time step.

The Christoffel symbols were calculated from an m-file developed by Down East Engineering (2014), which is available on the MathWorks File Exchange website. The code was analysed before being extensively tested on some common spacetime metrics, and successfully reproduced their corresponding Christoffel symbols.

3.5   Units

For interstellar space, SI units become quite cumbersome since large powers become involved. Through this thesis, the following length, time, and mass scales are used:

- Mass: $1\,M = 10^{10}\,M_\odot \approx 1.99 \times 10^{41}\,\text{kg}$
- Length: $1\,L = 1\,\text{kpc} \approx 3.09 \times 10^{19}\,\text{m}$
- Time: $1\,T = 1\,\text{kyr} \approx 3.16 \times 10^{10}\,\text{s}$

Some common constants and conversions that will be used throughout are shown below:

- $c = 3 \times 10^8\,\text{m s}^{-1} = 0.3068\,\text{kpc kyr}^{-1}$
- $G = 6.674 \times 10^{-11}\,\text{m}^3\,\text{kg}^{-1}\,\text{s}^{-2} = 4.500 \times 10^{-8}\,\text{kpc}^3\,\text{M}^{-1}\,\text{kyr}^{-2}$
- $g = 9.81\,\text{m s}^{-1} = 316.61\,\text{kpc kyr}^{-2}$
- $1\,\text{km s}^{-1} = 1.0227 \times 10^{-6}\,\text{kpc kyr}^{-1}$

3.6   Testing the Mass Model

To test the ODE's, the orbit of the Sun was calculated and compared with published results. The Sun orbits the galactic core of the Milky Way at a distance r_0 of roughly $8.5\,\text{kpc}$, velocity v_0 of about $220\,\text{km s}^{-1}$ (Kerr and Lynden-Bell, 1986), and an orbital period of roughly 220 Myr (Seeds and Backman, 2015), though exact figures will vary slightly in literature depending on the method used. The Sun's orbit is roughly elliptical, and oscillates up and down relative to the galactic plane (Moore and Rees, 2011). Throughout this research, we will assume that the Sun lies and stays within the galactic plane.

The initial coordinates of the Sun are set at

$$x^\alpha = (0, 0, -r_0, 0) \tag{3.32}$$

and the initial four-velocity is

$$u^\alpha = (u^t, -v_0, 0, 0) \tag{3.33}$$

where u^t is determined from Equation (3.30). The mass of the Sun is irrelevant in this calculation, and a^t and a_s are set to zero. A plot of the calculated orbit after $220\,\mathrm{Myr}$ is shown in Fig. 3.3, where the inner and outer dotted circles represent the size of the bulge and disk respectively. The final position of the Sun is indicated by the orange cross, and the final velocity vector is indicated by the orange arrow. An event was set up to determine the calculated orbital period of the Sun, as indicated by the orange circle. The orbital period of the Sun was found to be $203\,\mathrm{Myr}$, which is an acceptable value.
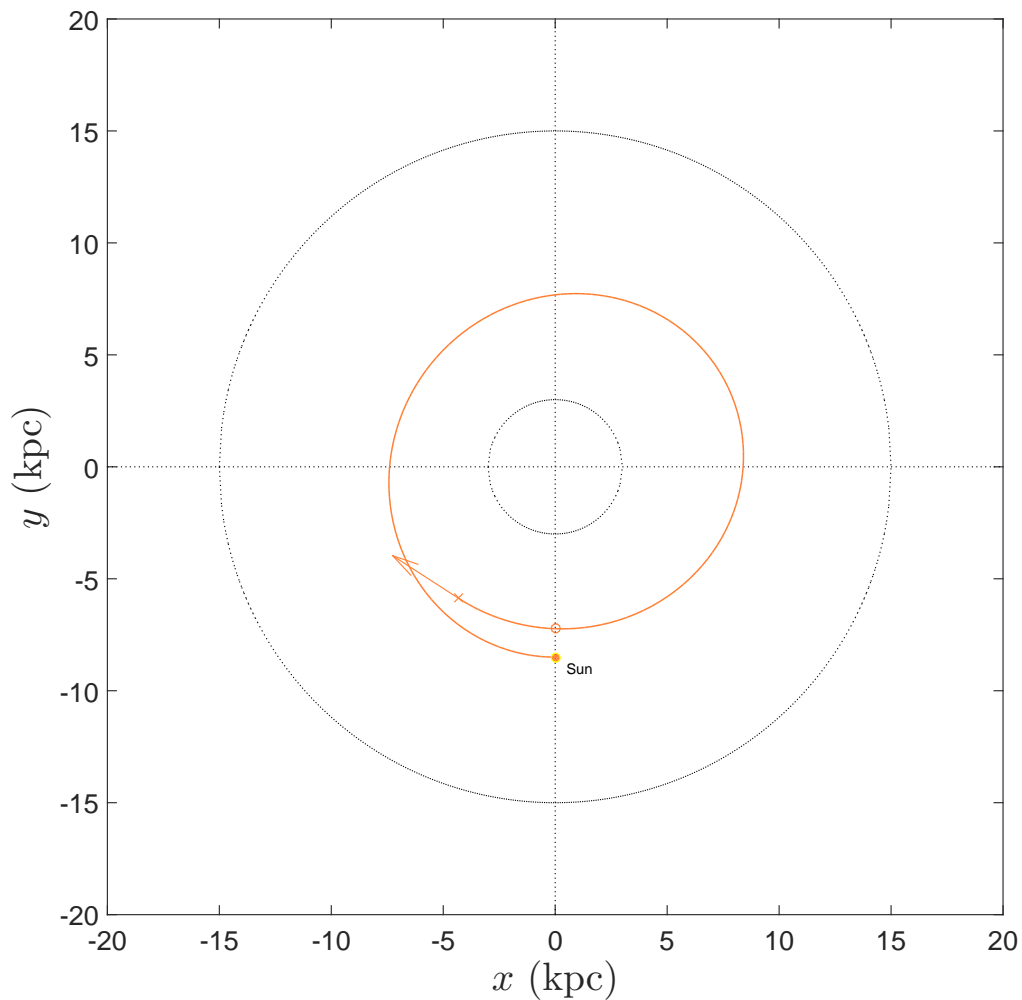

Figure 3.3: Calculated trajectory of the Sun.

Chapter 4

Genetic Algorithms

Now that we have all the machinery to calculate rocket trajectories, the next task is to find an optimal solution. A genetic algorithm is employed to determine the optimal trajectory. This chapter introduces the theory behind genetic algorithms, and concludes with a demonstration of the algorithm to solve an example problem.

4.1   Optimisation Methods

When approaching an optimisation problem, many types of optimisation methods can be employed, each offering unique advantages as well as disadvantages. Betts (1998) explored various numerical optimisation methods commonly used in trajectory problems, and compared the benefits of each; Vinkó and Izzo (2008) explored different optimisation methods to solve several spacecraft trajectory problems, and concluded that the most accurate solutions are produced by a combination of different solvers.

For this research task, the accuracy of the solution will depend on the gravitational model being used. Since the exact mass and size parameters of the Milky Way are still open to debate, a highly accurate global optimal solution would be unnecessary and meaningless. Rather, a simple optimisation algorithm will suffice, since we are only concerned with calculating an approximate optimal trajectory.

From the wide range of possible optimisation methods that could be employed, a genetic algorithm was chosen for several reasons. Genetic algorithms are simple to implement and heuristic, which is ideal for the given problem since we are only concerned with an approximate optimal solution. They also do not depend on any derivatives and their respective matrices like most other optimisation methods, making them computationally inexpensive to run. Charbonneau (1995) explored the use of genetic algorithms in astronomy and astrophysics to solve a variety of problems, and demonstrates their simplicity and robustness when compared with conventional optimisation techniques.

4.2   Theory

The motivation behind the development of genetic algorithms stems from our understanding behind the success of life on Earth. The algorithm effectively mimics the process of biological evolution and natural selection, whereby the fittest members of a species survive, and weak members that do not survive are removed from the genetic pool (Darwin, 1859). As a result, breeding tends to occur amongst its fittest members, which leads to offspring with desirable characteristics from each parent. The species is thus able to increase its chances of survival by continuously evolving. To simulate the genetic process, we start with an initial sample size and gradually evolve it toward the optimal solution (Coley, 1999):

1. A random population is first constructed, representing the first generation of the species.
2. The fitness of each member of the species is evaluated.
3. The second generation of the population is created by selecting the fittest members of the first generation, with breeding also occurring between the fittest members.
4. A mutation is randomly introduced into certain members to create genetic diversity.
5. Steps 2 to 5 are repeated for each subsequent generation.

The initial population is simply a set of random initial solutions, which we hope to evolve into a more accurate set of solutions. The quality of each solution is determined by a function f, known as the *fitness function*, which quantitatively determines the quality of each solution. The next generation of solutions is obtained by combining (*crossover*) and keeping (*selection*) the high quality solutions from the previous generation. The fittest member is always carried over onto the next generation (*elitism*) to ensure that the highest quality solution of the next generation will not be reduced. Slight changes are then introduced to this new set of solutions to expand the possible search space (*mutation*). This process of selection, crossover, and mutation, is usually continued until the fitness function reaches a specified value, or until a certain number of generations have passed.

4.3   Computational Approach

We are required to find an optimal solution to a problem with n variables, $x_1, x_2, \ldots, x_n$, such that the fitness function $f(x_1, \ldots, x_n)$ is minimised. A genetic algorithm will be used where each generation has a sample size m, and the i-th solution sample is denoted by $y_i = \begin{bmatrix} x_{i1} & x_{i2} & \ldots & x_{in} \end{bmatrix}$.

To begin, we first place limits on each variable x_j such that $x_{j,\min} \leq x_j \leq x_{j,\max}$, where $x_{j,\min}$ and $x_{j,\max}$ are the lower and upper limits of the variable x_j, respectively. To simulate the genetic process, each parameter x_{ij} in the solution sample is associated with a binary string X_{ij} of length ℓ, which has an equivalent decimal integer α_{ij}. Note that

the maximum decimal value of the binary string is $2^\ell - 1$, and hence $0 \leq \alpha_{ij} \leq 2^\ell - 1$. The binary strings are then mapped to a particular value of each variable:

$$x_{ij} = x_{j,\min} + \frac{\alpha_{ij}}{2^\ell - 1}(x_{j,\max} - x_{j,\min}) \tag{4.1}$$

Each solution sample is then represented by a single binary string, which consists of the individual binary strings of each variable. The binary string of the solution sample, which has a length $n\ell$, is denoted by $Y_i = \begin{bmatrix} X_{i1} & X_{i2} & \ldots & X_{in} \end{bmatrix}$. Each generation is therefore represented by a set of m binary strings.

To create the first generation of binary strings, we generate m random integer values between 0 and $2^\ell - 1$ for each of the n variables, and use Matlab's `dec2bin` function to convert them into binary strings. Each integer value is also mapped to the solution space using Equation (4.1). The fitness f_i is calculated for each solution sample y_i, which are then ranked in decreasing order of fitness, such that the highest quality (lowest fitness[1]) solutions are at the bottom of the list. The binary solution samples Y_i are also ranked accordingly. The best solution sample of that generation is then passed on to the next generation of solutions.

The remaining population is chosen randomly from either a selection or recombination process. The probability of selection and recombination are denoted by p_s and p_r, respectively, where $p_r = 1 - p_s$. The value of these parameters is determined from a sensitivity analysis. Matlab's `rand` function is used to generate a pseudorandom value from a standard uniform distribution. If the value is less than p_s, then selection will occur; if it is greater than p_s, then recombination will occur. In both cases, solution samples are chosen from a linear probability distribution, with higher quality solutions (at the bottom of the ranked list) more likely to be chosen over lower quality solutions (at the top of the ranked list). To generate a psuedorandom value from a linear distribution, we need to relate the uniform and linear probability distributions.

4.3.1   Linear Probability Distribution

The probability P_0 of choosing a number less than x between 0 and 1 using a uniform probability distribution is simply

$$P_0(x) \equiv P_0(< x) = \int_0^x dx' = x \tag{4.2}$$

---

[1]By "lowest fitness", we actually mean lowest fitness value as determined by f.

Likewise, the probability P_1 of choosing a number less than y between 0 and 1 using a linear probability distribution P_1 is given by

$$P_1(y) \equiv P_1(< y) = 2 \int_0^y y' \, dy' = y^2 \tag{4.3}$$

The two probability distributions are therefore related through $y = \sqrt{x}$. For psuedorandom values between 0 and n, the relationship is simply

$$y = n\sqrt{x} \tag{4.4}$$

Fig. 4.1 shows a histogram of 10000 random values chosen between 0 and 100 based on uniform and linear distributions.

By generating psuedorandom integer values between 0 and n (our sample size) using a linear probability distribution, higher quality solutions for selection and recombination are more likely to be chosen from the solution samples.
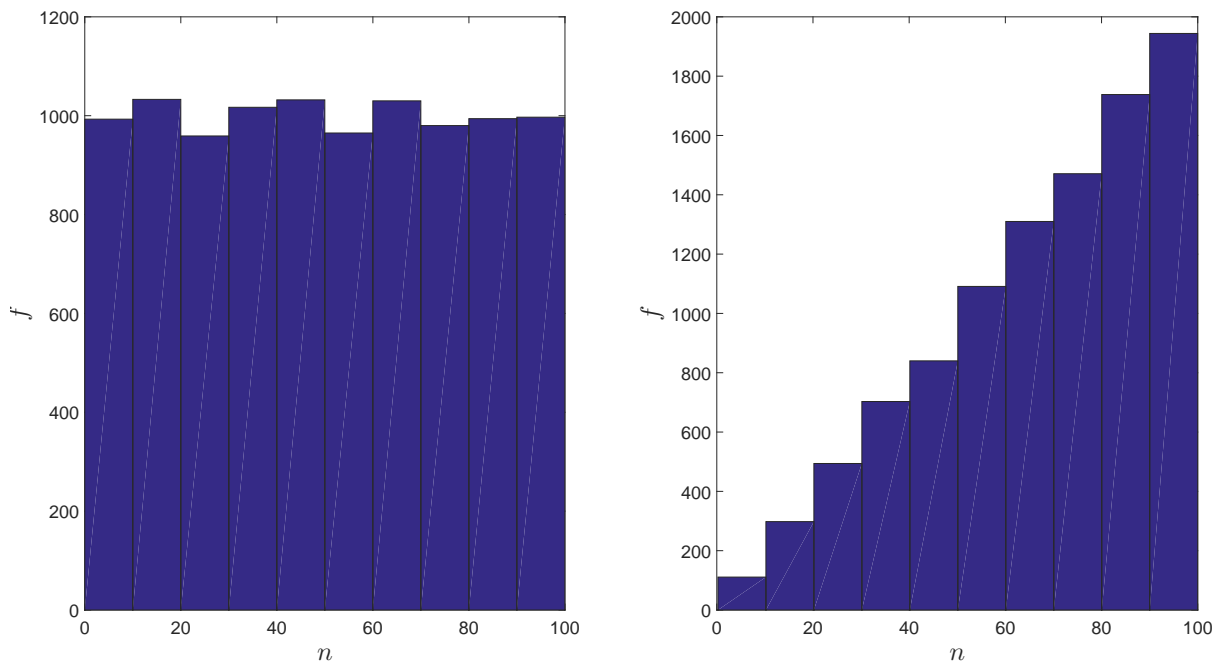
Figure 4.1: Uniform (left) and linear (right) probability distributions.

4.3.2 Selection, Recombination, Mutation

Selection is straight forward, and works in the same manner as elitism where the solution sample Y_i chosen from a linear probability distribution is carried over to the next generation.

Recombination requires two solution samples to be chosen from a linear probability distribution. Once these two solutions, Y_a and Y_b, are chosen, then they can be combined.

First, a random digit location k is chosen where both solution strings are split. This random digit location is chosen from a uniform distribution of integers between 1 and $n\ell - 1$ (the number of possible places to cut the binary string). The first string section of Y_a is combined with the second string section of Y_b, and vice versa. This recombination process produces two new solutions Y_{ab} and Y_{ba}:

$$Y_{ab} = [Y_a(1{:}k) \quad Y_b(k + 1{:}n\ell - 1)] \tag{4.5}$$

$$Y_{ba} = [Y_b(1{:}k) \quad Y_a(k + 1{:}n\ell - 1)] \tag{4.6}$$

where $Y_i(a{:}b)$ refers to all the binary digits between, and including, the a-th and b-th digits of the solution sample Y_i.

Once selection or recombination is chosen, the solution sample(s) have a chance to mutate. A psuedorandom value from a uniform probability distribution is generated, and if this value is less than the mutation probability, p_m, then the solution sample will undergo a slight modification. A random digit location q from the binary string Y_i is chosen from a uniform distribution of integers between 1 and $n\ell$ (the length of each binary string). To simulate the mutation process, the binary digit at this digit location is then flipped, so that:

$$Y_i(q) = \begin{cases} 1 & \text{if } Y_i(q) = 0 \\ 0 & \text{if } Y_i(q) = 1 \end{cases} \tag{4.7}$$

where $Y_i(q)$ refers to the q-th binary digit of the solution sample Y_i.

The process of selection, recombination, and mutation is repeated until we have the next generation of m solution samples. The new binary strings of each parameter are then extracted from the solution sample Y_i, and these are converted back to decimal values using Matlab's `bin2dec` function and Equation (4.1). The fitness is then calculated for each solution sample of this new generation, and these new solution samples are ranked in order of decreasing fitness. The binary solution samples are ranked accordingly, and the most elite solution sample is carried over without any mutations. The next generation is then created by applying the selection, recombination, and mutation genetic operators onto solution samples chosen from a linear probability distribution. This entire process is repeated until a set number of generations have passed, or the fitness satisfies some convergence criterion.

As mentioned previously, genetic algorithms are unable to find globally optimal solutions since they are heuristic in nature. As no optimality conditions are specified, the "optimal" solutions found are merely solutions that are better than the rest. The effectiveness of the algorithm depends on the sample size as well as the various evolution parameters described above, which are unique to each problem. Refining these parameters is done through a sensitivity analysis, that is, significant trial-and-error testing. The

final solution quality is also heavily dependent on the quality of the initial batch of solutions, with high quality batches typically leading to an optimal solution very quickly, and bad quality batches possibly leading to very poor final solutions. Hence, better results are achieved with a larger sample size, though this will limit the computational speed of the algorithm. Alternatively, a smaller sample size will speed up the computation, but may require even a finely-tuned algorithm to be run several times before a viable optimal solution is found, though this will depend on the dimensions of the given problem. The accuracy of the solution can be improved by increasing the resolution of each parameter. The resolution $x_{j,\mathrm{res}}$ of parameter x_j is

$$x_{j,\mathrm{res}} = \frac{x_{j,\mathrm{max}} - x_{j,\mathrm{min}}}{2^\ell - 1} \tag{4.8}$$

A finer resolution can be obtained by increasing the number of digits of the binary strings. However, doing so usually requires a longer computational time before convergence, since there are more string locations that can be cut and mutated. This trade-off between solution accuracy and computational time needs to be considered in any problem. Alternatively, an initial approximate optimal solution can first be found by running the genetic algorithm with a low resolution, and can then be refined by increasing the resolution at a later stage.

4.4 Testing the Algorithm

Consider a projectile fired from the origin with an initial velocity v at an angle θ to the horizontal. We require that the projectile reach the top of a cliff with coordinates (x_f, y_f), and we aim to find the optimal solution (v_0, θ_0) such that the projectile reaches the required coordinate with the minimum final velocity v_f.

We now test the genetic algorithm on this example problem, and compare it with the analytical result.

4.4.1 Analytical solution

The equations of motion are given by

$$x(t) = vt \cos \theta \tag{4.9}$$

$$y(t) = vt \sin \theta - \frac{1}{2}gt^2 \tag{4.10}$$

where t is the time coordinate. Combining the above two equations leads to

$$y(x) = x \tan \theta - \frac{gx^2}{2v^2} \sec^2 \theta \tag{4.11}$$

By setting $y(x_f) = y_f$, it can be shown that

$$v^2 = \frac{gx_f^2 \sec^2 \theta}{2\left(x_f \tan \theta - y_f\right)} \tag{4.12}$$

The velocity components at (x_f, y_f) is given by:

$$\dot{x}_f = v \cos \theta \tag{4.13}$$
$$\dot{y}_f = v \sin \theta - gt_f \tag{4.14}$$

where t_f is the time it takes to reach (x_f, y_f). By setting $x(t_f) = x_f$, Equation (4.14) can then be rewritten as

$$\dot{y}_f = v \sin \theta - \frac{gx_f}{v \cos \theta} \tag{4.15}$$

The final velocity magnitude v_f is simply

$$v_f^2 = \dot{x}_f^2 + \dot{y}_f^2 \tag{4.16}$$

which leads to the result

$$v_f^2 = v^2 - 2gy_f \tag{4.17}$$

The minimum final velocity occurs when

$$\left.\frac{dv_f^2}{d\theta}\right|_{\theta=\theta_0} = 0 \tag{4.18}$$

Solving the above equation for the optimal angle θ_0 leads to

$$\tan \theta_0 = \frac{y_f \pm \sqrt{y_f^2 + x_f^2}}{x_f} \tag{4.19}$$

The positive square root is then taken since $0 < \theta_0 < \dfrac{\pi}{2}$, which implies that $\tan \theta_0 > 0$. The second derivative of v_f was also calculated to be

$$\left.\frac{d^2 v_f}{d\theta^2}\right|_{\theta=\theta_0} > 0 \tag{4.20}$$

which shows that the v_f is indeed a minimum (rather than a maximum) at θ_0.

The optimal initial velocity v_0 is found by substituting the above result into Equation

(4.12), which leads to

$$v_0 = \sqrt{g \left(\sqrt{x_f^2 + y_f^2} + y_f \right)}$$ (4.21)

The minimum final velocity is calculated from Equation (4.17) to be

$$v_f = \sqrt{g \left(\sqrt{x_f^2 + y_f^2} - y_f \right)}$$ (4.22)

4.4.2   Using the Genetic Algorithm

The same problem is now solved using a genetic algorithm with 2 variables (the initial velocity and angle). The coordinates of the edge of the cliff are chosen to be (8,4), which leads to the analytical results:

$$v_0 = 11.27 \, \mathrm{m \, s^{-1}}$$ (4.23)
$$\theta_0 = 58.28°$$ (4.24)
$$v_f = 6.96 \, \mathrm{m \, s^{-1}}$$ (4.25)

The fitness function to be minimised is

$$f = (x_f - x)^2 + (y_f - y)^2 + k_v v^2$$ (4.26)

where k_v is the velocity weighting factor. The fitness for each solution sample is calculated at each point along the trajectory, and the minimum fitness along that path is taken to be the fitness for that solution. The accuracy of the solution can therefore be improved by increasing the number of points used in the integration, so that the fitness is assessed at finer intervals. For this problem, the number of points is increased by a factor of 100, which is 25 times more than the default number of points used in the `ode45` function.

For the fitness calculation, we set $k_v = 0.01$, leading to a minimum fitness $f_{\min}$ of

$$f_{\min} = 0.485$$ (4.27)

The algorithm is set to terminate after 100 generations, and the parameters chosen for the genetic algorithm are shown in Table 4.1. The following bounds were placed on the initial velocity and angle:

$$\begin{aligned} v_{0,\min} &= 0 \, \mathrm{m \, s^{-1}} \quad v_{0,\max} = 20 \, \mathrm{m \, s^{-1}} \\ \theta_{0,\min} &= 0° \qquad\qquad \theta_{0,\max} = 90° \end{aligned}$$ (4.28)

The velocity and angular resolutions are calculated from Equation (4.8) to be

$$v_{\text{res}} = 0.020 \text{ m s}^{-1} \tag{4.29}$$

$$\theta_{\text{res}} = 0.088° \tag{4.30}$$

which is sufficiently accurate for this problem.

Parameter	Value
Binary digits ℓ	10
Sample size m	100
Selection probability p_s	25%
Mutation probability p_m	25%

Table 4.1: Genetic algorithm parameters.

The results produced by the algorithm are shown in Fig. 4.2. The fitness as a function of generation is shown in Fig. 4.2(a), where the dotted line represents the expected minimal fitness. It is clear that the optimal solution of each generation rapidly improves before plateauing off. The optimal solution is found at generation 22, where the fitness reaches 0.485 and stops decreasing. The minimum fitness of the optimal trajectory occurs at a distance of 0.012 m from the target coordinates. Fig. 4.2(b) compares the analytical solution (blue) with the solution found using the genetic algorithm (red), where the arrowheads represent the magnitude and direction of the final velocity vector. The optimal solution of the first generation (dotted black), which has been truncated at the point of minimal fitness, is also shown to illustrate the improvement after 22 generations. The optimal initial velocity $v_{0,\text{opt}}$, initial angle $\theta_{0,\text{opt}}$, and final velocity $v_{f,\text{min}}$ were calculated to be

$$v_{0,\text{opt}} = 11.26 \text{ m s}^{-1} \tag{4.31}$$

$$\theta_{0,\text{opt}} = 58.33° \tag{4.32}$$

$$v_{f,\text{min}} = 6.96 \text{ m s}^{-1} \tag{4.33}$$

Note that the calculated initial velocity and angle both lie within one resolution unit of the analytical solution, demonstrating that this is the most accurate solution given the existing parameters. A more accurate solution can be achieved by either improving the resolution of the variables (that is, by increasing the number of binary digits ℓ), or, to a minor extent, by increasing the number of points used in the integration.

4.5   Implementation

The genetic algorithm is now implemented into the Milky Way mass model to calculate the optimal trajectories given the maximum acceleration magnitude.
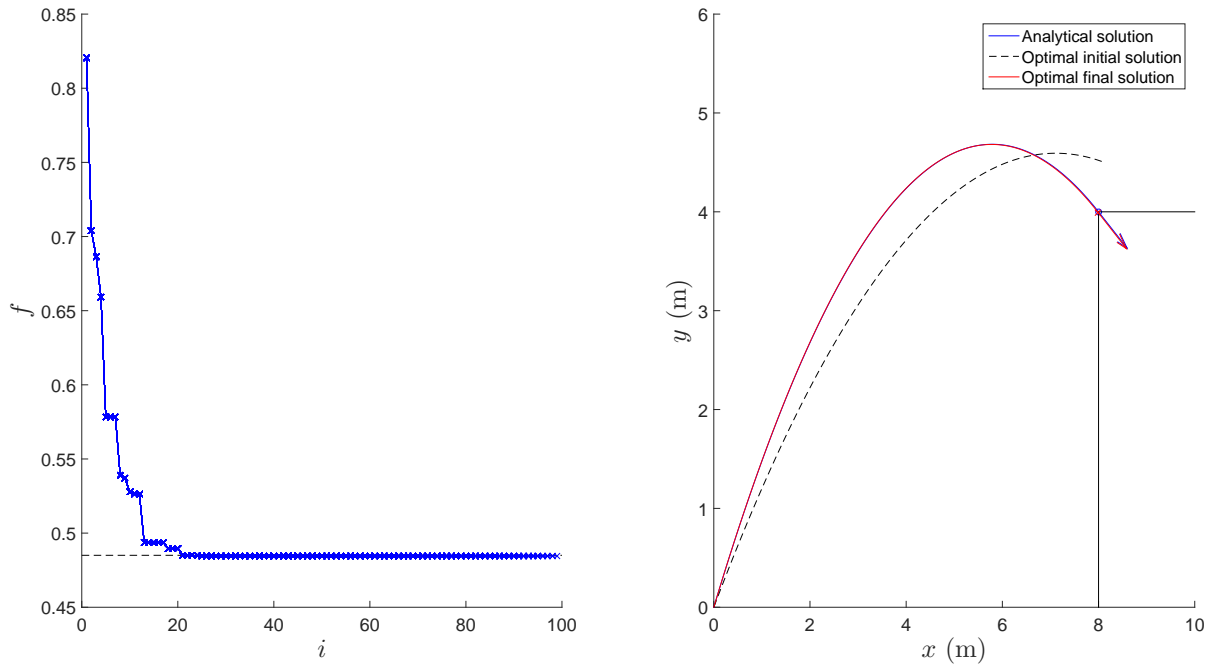
Figure 4.2: Fitness (left) and optimal trajectory (right) of example problem.

4.5.1   Spherical Coordinates

The equations of motion require four input variables from the rocket: the magnitude a of the four-acceleration, and the three components of the unit thrust vector (a_x, a_y, a_z). The unit thrust vector of the rocket can be simplified by using spherical coordinates, which depends on the inclination θ and azimuthal ϕ angles, where $0 \leq \theta \leq \pi$ and $0 \leq \phi \leq 2\pi$. The conversion between spherical and Cartesian unit vectors is given by

$$a_x = \sin\theta \cos\phi \tag{4.34}$$

$$a_y = \sin\theta \sin\phi \tag{4.35}$$

$$a_z = \cos\theta \tag{4.36}$$

Hence, there are now three variables which need to be solved by the genetic algorithm: (a, θ, ϕ). Each of these variables need to vary throughout the journey as a function of the proper time τ. To achieve this, a spline is fitted through n evenly spaced splines points of each variable between $\tau = 0$ and the final integration time τ_{end}. There is a total of $3n$ variables that need to be optimised by the genetic algorithm, where each solution sample contains the spline values in the form

$$y_i = [a_1 \quad \dots \quad a_n \quad \theta_1 \quad \dots \quad \theta_n \quad \phi_1 \quad \dots \quad \phi_n] \tag{4.37}$$

4.5.2   Boundary Conditions

The boundary conditions of the trajectories need to be set. The trajectories begin from Earth, with the same initial conditions as the Sun:

$$x^\alpha = (0, 0, -r_0, 0) \tag{4.38}$$

$$u^\alpha = (u^t, -v_0, 0, 0) \tag{4.39}$$

where $r_0 = 8.5\,\text{kpc}$, $v_0 = 220\,\text{km s}^{-1}$, and u^t is determined from Equation (3.30). A rocket arriving at a galactic destination (x_f, y_f, z_f) must also have the correct orbital velocity of the star system. Galactic rotation curves show that the orbital velocity as a function of radial distance is roughly constant outside the galactic bulge (Jones and Lambourne, 2004). For the Milky Way, the orbital velocity remains roughly constant around $220\,\text{km s}^{-1}$ outside a radius of about $3\,\text{kpc}$. Thus, the rocket must arrive at its final destination with a final speed v_f of $220\,\text{km s}^{-1}$, with four-velocity components

$$u_f^x = v_f \sin \phi_f \sin \theta_f \tag{4.40}$$

$$u_f^y = -v_f \cos \phi_f \sin \theta_f \tag{4.41}$$

$$u_f^z = -v_f \cos \theta_f \tag{4.42}$$

where the final angular positions θ_f and ϕ_f are given by

$$\phi_f = \tan^{-1} \frac{y_f}{x_f} \tag{4.43}$$

$$\theta_f = \cos^{-1} \frac{z_f}{\sqrt{x_f^2 + y_f^2 + z_f^2}} \tag{4.44}$$

The initial mass of the rocket is set to some arbitrary value. Once the optimal solution is found, the required mass is determined from Equation (3.17), and the equations of motion are recalculated using the required mass as the initial mass.

4.5.3   Fitness Function

The fitness function is given by

$$f = (x - x_f)^2 + (y - y_f)^2 + (z - z_f)^2 \tag{4.45}$$

$$+ k_v[(u^x - u_f^x)^2 + (u^y - u_f^y)^2 + (u^z - u_f^z)^2] + k_\tau \tau^2 \tag{4.46}$$

where k_v and k_τ are the velocity and proper time weighting factors, respectively. The fitness for each solution sample is calculated at each point along the trajectory, and the minimum fitness along that path is taken to be the fitness for that solution.

4.5.4   Variable Bounds

The bounds for each of the angular spline points are set to be

$$\theta_{\min} = 0 \quad \theta_{\max} = \pi$$
$$\phi_{\min} = 0 \quad \phi_{\max} = 2\pi \tag{4.47}$$

The lower and upper bounds on the spline points of the four-acceleration magnitude, $a_{\min}$ and $a_{\max}$, are chosen to be equal and opposite in magnitude, where a negative acceleration is equivalent to an acceleration in the opposite direction. Higher quality solutions are achieved if the acceleration limits are chosen in conjunction with the integration time. For example, suppose a rocket can reach a destination in 10 years, with an acceleration that varies linearly from 10^{-9} g to -10^{-9} g. It would be pointless to set the bounds of the acceleration to be ± 1 g and integrate over a period of 1 kyr. Such an attempt would yield extremely poor solutions unless: (a) an unreasonably large number of spline points were used (with spline points located at 10 year intervals); or (b) if an unreasonably large number of binary digits ℓ were used (resulting with an acceleration resolution on the order of 10^{-9} g). Increasing the number of spline points used in the integration becomes computationally expensive, considerably increasing the time it takes to calculate for the trajectory of each solution. Alternatively, significantly increasing the binary digits ℓ is impractical, and would cause convergence problems.

It should be noted that the bounds on the spline points do not prevent the variables from exceeding these bounds. A non-linear spline containing more than 2 spline points can exceed the limits placed on the actual spline points. For the angular variables, this is not an issue. However, this can become a problem for the acceleration magnitude for reasons described above. Consequently, strict limits are placed on the acceleration magnitude by ensuring that

$$a(\tau) = \begin{cases} a_{\min} & \text{if } a(\tau) < a_{\min} \\ a(\tau) & \text{if } a_{\min} \leq a(\tau) \leq a_{\max} \\ a_{\max} & \text{if } a(\tau) > a_{\max} \end{cases} \tag{4.48}$$

Now that the genetic algorithm has been implemented, it is time to consider galactic destinations.

Chapter 5

Results

This chapter outlines the results that were obtained using the genetic algorithm to calculate various optimal trajectories around the Milky Way using a low-acceleration rocket. To determine the viability of low-acceleration rockets to colonise the Milky Way, various target locations both within and outside the galactic disk are considered.

5.1   Rocket Parameters

The rocket mass and exhaust velocity has a significant role when it comes to choosing the type of propulsion system used for an interstellar journey. The values used will be based on expected technologies available in the future. Powell and Pelligrino (1987) designed a manned theoretical spacecraft that could accelerate up to relativistic velocities. This spacecraft, named Project Valkyrie, used matter-antimatter annihilation as its source of propulsion. The spacecraft had a unique design, resulting in a relatively low mass of 100 tons without fuel. This is comparable to the mass of the Space Shuttle Orbiter and less than the International Space Station.

When travelling to distant star systems, interstellar journeys are likely to require a multi-generational spacecraft. The mass of the interstellar spacecraft used for the trajectory calculation will be roughly based on Project Valkyrie. The mass of the spacecraft (without fuel) is set to 1000 tons to account for a multi-generational journey. It should be noted that the actual empty mass of the spacecraft is not really important; rather, we are more concerned with the fuel-to-empty rocket mass ratio β. When calculating this ratio, three sources of propulsion will be considered:

- Fusion rocket: Fusion rockets utilise the process of nuclear fusion to propel the spacecraft forward. One form of fusion technology is nuclear pulse propulsion, which works by detonating nuclear devices behind the spacecraft, and can achieve effective exhaust velocities of up to $15{,}000\,\mathrm{km\,s^{-1}}$ (Matloff, 2010). The fusion rocket here will utilise nuclear pulse propulsion with an effective exhaust velocity of $10{,}000\,\mathrm{km\,s^{-1}}$.

- Antimatter rocket: Proton-antiproton annihilation is extremely efficient, and can convert more than 50% of the fuel mass to usable exhaust kinetic energy with an effective exhaust velocity of up to $0.67c$ (Matloff, 2010). For the antimatter drive used here, an effective exhaust velocity of $0.5c$ is used for the reaction products of the proton-antiproton reaction.
- Photon rocket: A photon rocket is an ideal rocket that generates thrust by emitting photons generated through electron-positron annihilation[1], and thus has an exhaust velocity equal to the speed of light (Tinder, 2006).

5.2 Optimal Trajectories

Various final destinations around the Milky Way are considered:

- A. Star systems located within the galactic plane.
- B. Hypervelocity stars in the galactic plane.
- C. Star systems in the galactic halo.

For each of the above scenarios, three different locations are chosen:

1. Located near the Sun in the 3rd quadrant[2].
2. Located further from the Sun in the 2nd quadrant.
3. Located in the 4th quadrant, requiring the rocket to perform a complete turnaround before aligning itself with the velocity vector of the star.

Recall that the objective is not to find exact trajectory solutions to a the destinations. Rather, the goal is to determine the viability of a given propulsion system to reach a destination in a reasonable amount of time for the onboard travellers. As such, a few assumptions are made to simplify the analysis, which are outlined below.

For each destination, we aim to arrive within $0.2\,\mathrm{kpc}$ and within $20\,\mathrm{km\,s^{-1}}$ of the target destination. Note that star systems further away from the galactic center will take longer to complete their orbit, and hence their distance from the Sun could change appreciably with time. We have assumed that upon arrival, the location of each star system remains unchanged relative to the Sun. This assumption is reasonable as long as the time taken to reach the destination is significantly shorter than the period of the orbit. An integration period of $1\,\mathrm{Myr}$ is used in the calculations, which is a relatively short time span in galactic orbits (recall that the period of the Sun is about $220\,\mathrm{Myr}$).

We will assume that star systems in the galactic disk lie within the galactic plane,

---

[1]While photon rockets are a type of antimatter rocket, we will use the term "antimatter rocket" to refer to proton-antiproton annihilation, and "photon rocket" to refer to electron-positron annihilation.

[2]The quadrants are defined with the same convention as the Cartesian plane for $z = 0$, so that the first quadrant corresponds to $x, y > 0$.

which is a reasonable assumption since the average width of the disk is about 1% of the diameter of the disk. Thus, we can further simplify the analysis by setting $\theta = \pi/2$ throughout the calculation, so that there are only $2n$ variables that need to be optimised. To ensure that the inclination angle remains unchanged, the lower and upper bounds are set to $\pi/2$. The inclination angle spline points can then be disregarded during recombination and mutation by removing the possible binary digit locations from the psuedorandom generator.

The following parameters used in each scenario are shown in Table 5.1. With 10 binary digits, the angular resolutions are

$$\theta_{\mathrm{res}} = 0.18° \tag{5.1}$$

$$\phi_{\mathrm{res}} = 0.35° \tag{5.2}$$

In each scenario, the genetic algorithm is run 20 times, and the solution with the lowest final fitness is presented.

Parameter	Value
Binary digits	10
Sample size	200
Generations	100
Selection probability	25%
Mutation probability	25%
Spline points	2
Velocity weighting factor	10^{-5}
Proper time weighting factor	10^{-2}

Table 5.1: Parameters of the GA used in the interstellar trajectory calculation.

For the low-acceleration rocket considered here, the lower and upper acceleration limits are chosen to be $\pm 10^{-5}$ g, leading to an acceleration resolution of

$$a_{\mathrm{res}} = 1.96 \times 10^{-9}\,\mathrm{g}. \tag{5.3}$$

5.2.1   Destination A1: The Galactic Plane

The first star system is located within the galactic plane at $(-7, -5, 0)$, about $8\,\mathrm{kpc}$ from the Sun. Fig. 5.1(a) plots the fitness as a function of generation. Fig. 5.1(b) plots the optimal trajectory (red) and the trajectory of the Sun (orange) during this time, where the arrows represent the calculated (red) and required (blue) final velocity vector. The final position and three velocity deviations were calculated to be $0.09\,\mathrm{kpc}$ and $23\,\mathrm{km\,s^{-1}}$ respectively.

Fig. 5.2 shows the various parameters of the optimal trajectory as a function of proper

time. The left column plots the variables a, θ, and ϕ over the entire integration period, where the dotted lines represent the lower and upper limits of each variable. The middle column plots these same variables, but are truncated at the point of minimum fitness (that is, at the end of the trajectory). The right column plots the velocity function (top), mass function (middle)[3], and normalisation values (bottom). During this journey, a maximum velocity of $0.11c$ was reached, and required a total proper time of $351\,\mathrm{kyr}$. The fuel-to-empty rocket mass ratio β for each propulsion system is shown in Table 5.2.

Propulsion system	β
Fusion rocket	615
Antimatter rocket	0.53
Photon rocket	0.24

Table 5.2: Fuel-to-empty rocket mass ratio to destination A1.
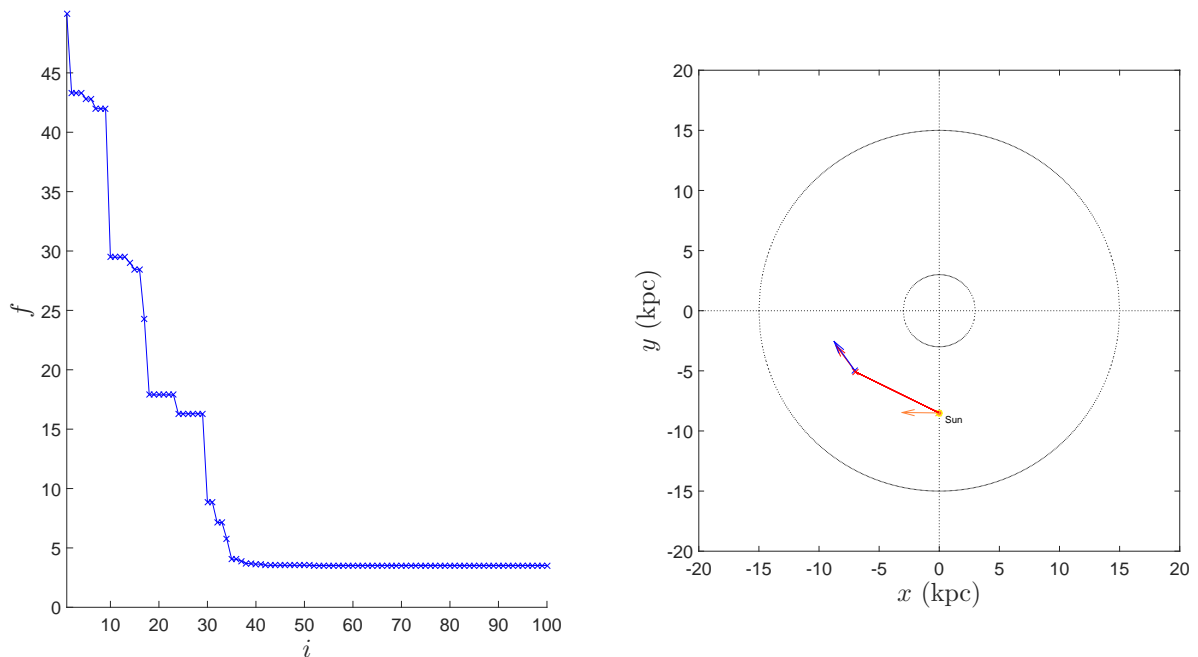
Figure 5.1: Fitness (left) and optimal trajectory (right) to destination A1.

5.2.2 Destination B1: A Hypervelocity Star

Hypervelocity stars (HVS) are stars with abnormally large velocities that exceed the escape velocity of the galaxy, travelling on radial paths with velocities exceeding $1000\,\mathrm{km\,s^{-1}}$ (Baumgardt et al., 2006). These stars are believed to originate from the core of galaxies, where supermassive blackholes are thought to exist (Hills, 1988). Reaching a hypervelocity star is of interest if one wishes to leave the galaxy, as orbiting around these stars

---

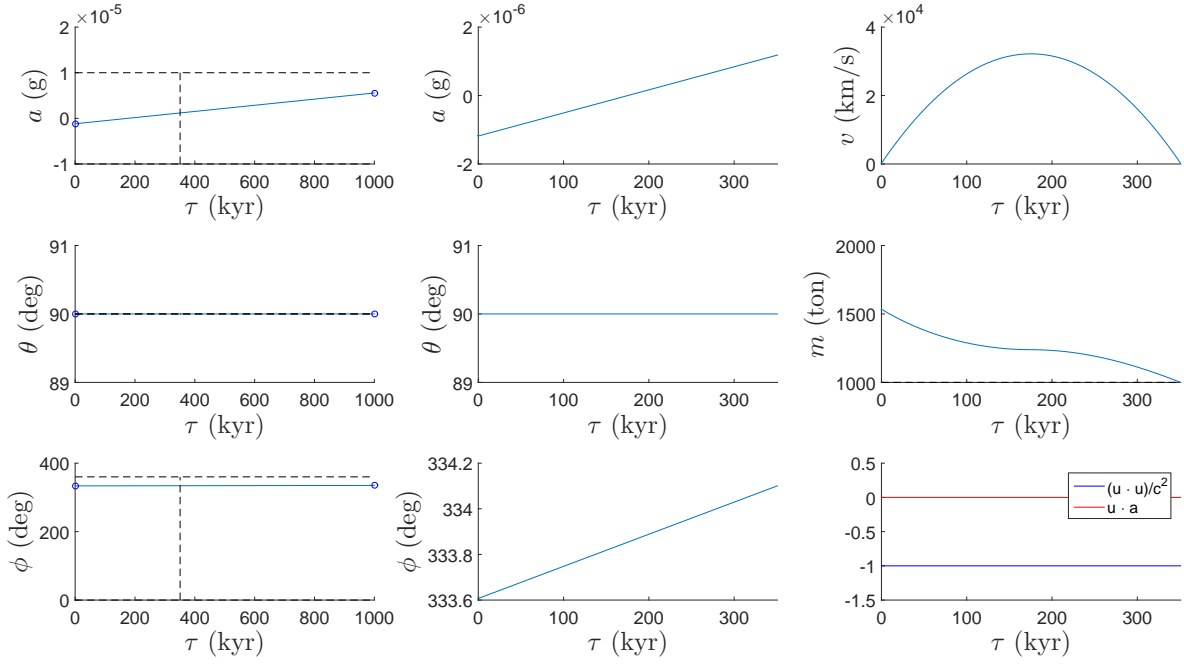[3]The mass functions shown in each scenario are for the antimatter rocket.

Figure 5.2: Parameters of the trajectory to destination A1.

provides a means of collecting energy during the journey. For a star on a radial trajectory, the velocity components are

$$u_f^x = v_f \cos\phi_f \sin\theta_f \tag{5.4}$$

$$u_f^y = v_f \sin\phi_f \sin\theta_f \tag{5.5}$$

$$u_f^z = v_f \cos\theta_f \tag{5.6}$$

where the final angular coordinates are given by Equation (4.43) and (4.44).

We now use the genetic algorithm to determine the optimal trajectory to reach a HVS located at $(-9, -4, 0)$, about $10\,\mathrm{kpc}$ from the Sun, and with a velocity magnitude of $2000\,\mathrm{km\,s^{-1}}$.

The results are shown in Fig. 5.3 and 5.4. The final position and three velocity deviations were calculated to be $0.17\,\mathrm{kpc}$ and $33\,\mathrm{km\,s^{-1}}$ respectively. During this journey, a maximum velocity of $0.12c$ was reached, and required a total proper time of $390\,\mathrm{kyr}$. The fuel-to-empty rocket mass ratio β for each propulsion system is shown in Table 5.3.

Propulsion system	β
Fusion rocket	1349
Antimatter rocket	0.62
Photon rocket	0.27

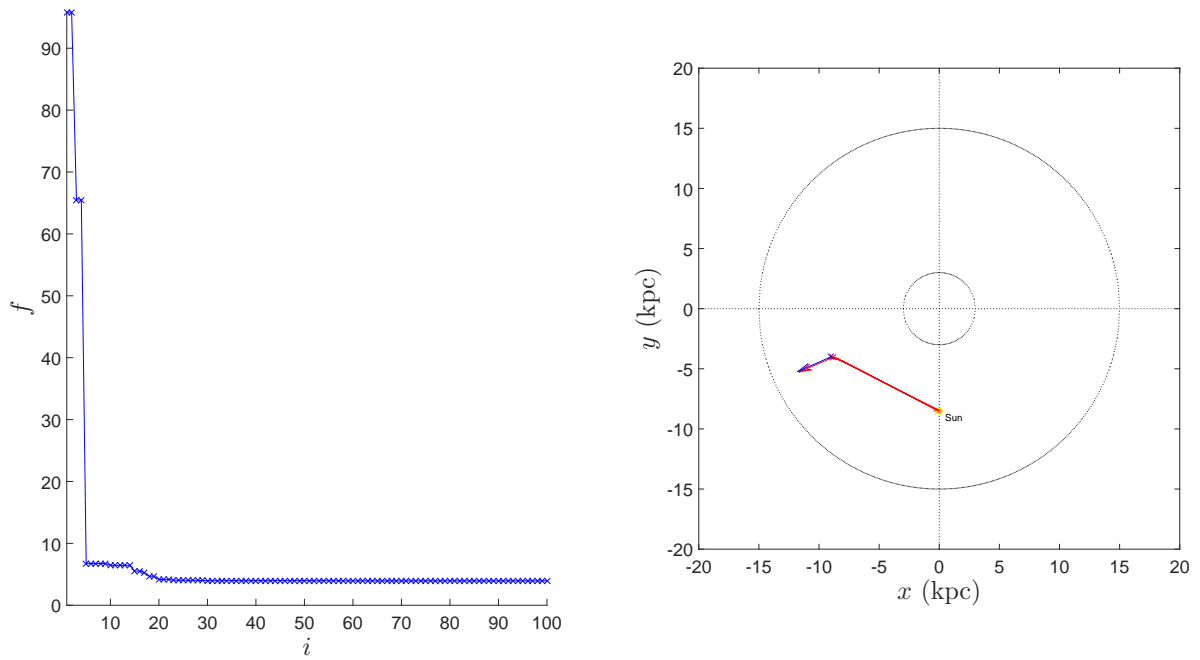Table 5.3: Fuel-to-empty rocket mass ratio to destination B1.

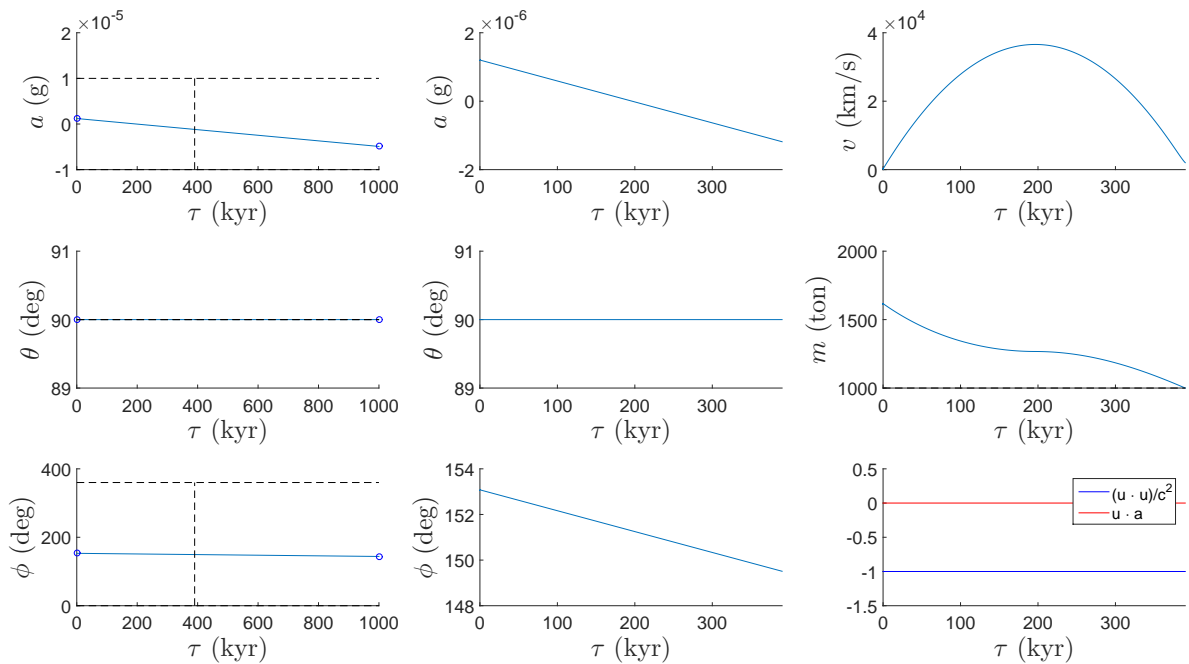Figure 5.3: Fitness (left) and optimal trajectory (right) to destination B1.

Figure 5.4: Parameters of the trajectory to destination B1.

5.2.3 Destination C1: The Galactic Halo

The third star system chosen will lie in the galactic halo to determine if the genetic algorithm can solve for the extra angular variable θ. The star system chosen is located at $(-6, -5, 2)$, about $7\,\text{kpc}$ from the Sun. The results are shown in Fig. 5.5 to 5.7. The

final position and three velocity deviations were calculated to be $0.73\,\mathrm{kpc}$ and $10\,\mathrm{km\,s^{-1}}$ respectively. During this journey, a maximum velocity of $0.10c$ was reached, and required a total proper time of $328\,\mathrm{kyr}$. The fuel-to-empty rocket mass ratio β for each propulsion system is shown in Table 5.4.

Propulsion system	β
Fusion rocket	493
Antimatter rocket	0.51
Photon rocket	0.23

Table 5.4: Fuel-to-empty rocket mass ratio to destination C1.
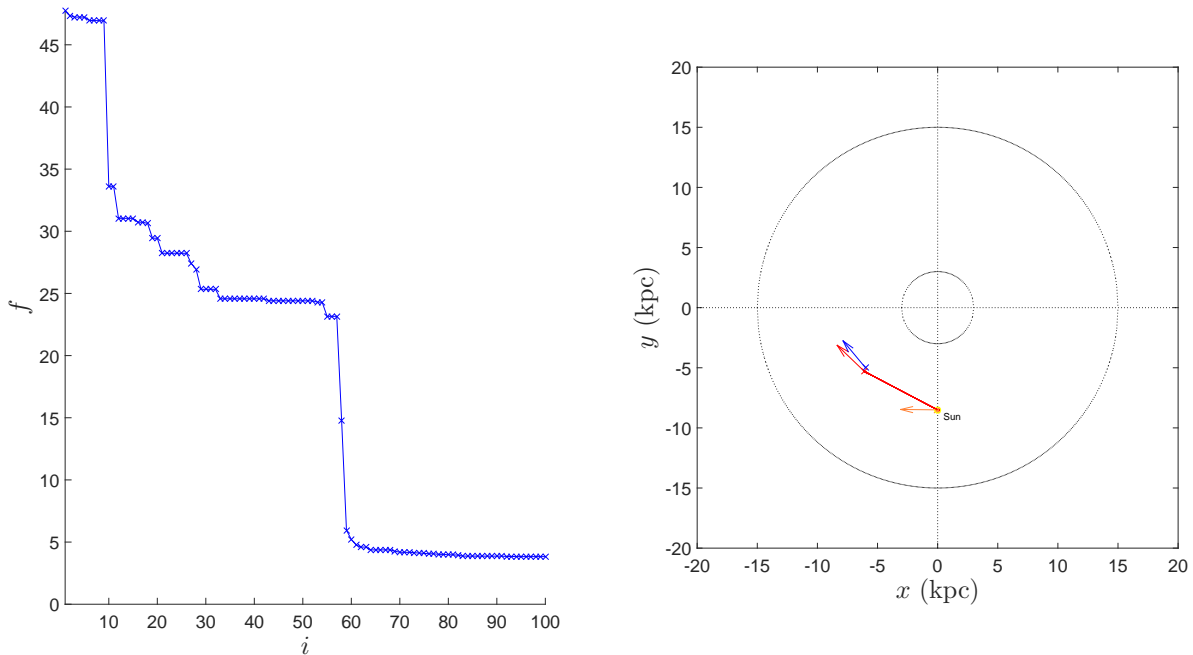
Figure 5.5: Fitness (left) and optimal trajectory (right) to destination C1.

5.2.4   Destination A2: The Galactic Plane

The next star system in the galactic plane is located at $(-10, 3, 0)$, about $15\,\mathrm{kpc}$ from the Sun. The results are shown in Fig. 5.8 and 5.9. The final position and three velocity deviations were calculated to be $0.24\,\mathrm{kpc}$ and $12\,\mathrm{km\,s^{-1}}$ respectively. During this journey, a maximum velocity of $0.19c$ was reached, and required a total proper time of $377\,\mathrm{kyr}$. The fuel-to-empty rocket mass ratio β for each propulsion system is shown in Table 5.5.

5.2.5   Destination B2: A Hypervelocity Star

The second HVS is located at $(-15, 5, 0)$, about $20\,\mathrm{kpc}$ from the Sun, and with a velocity magnitude of $2000\,\mathrm{km\,s^{-1}}$. The results are shown in Fig. 5.10 and 5.11. The final position
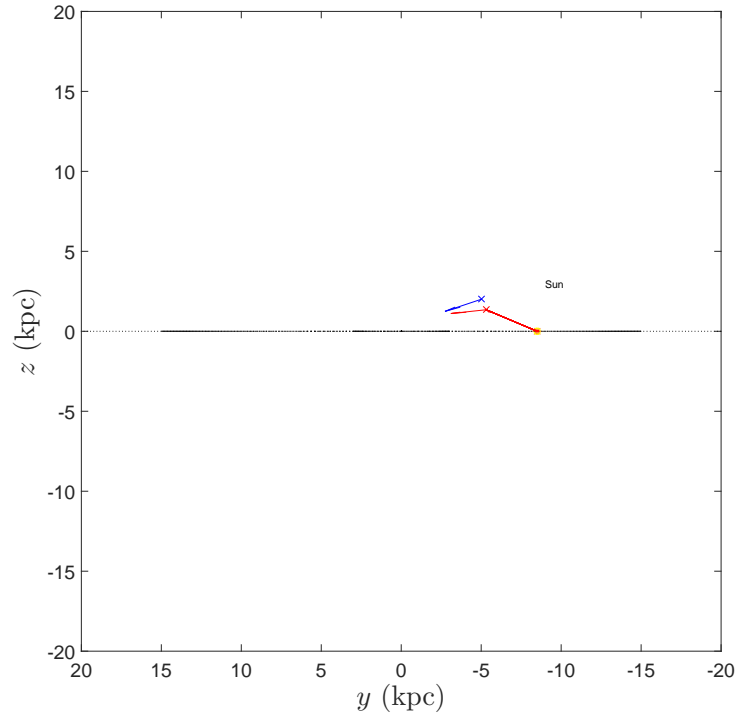
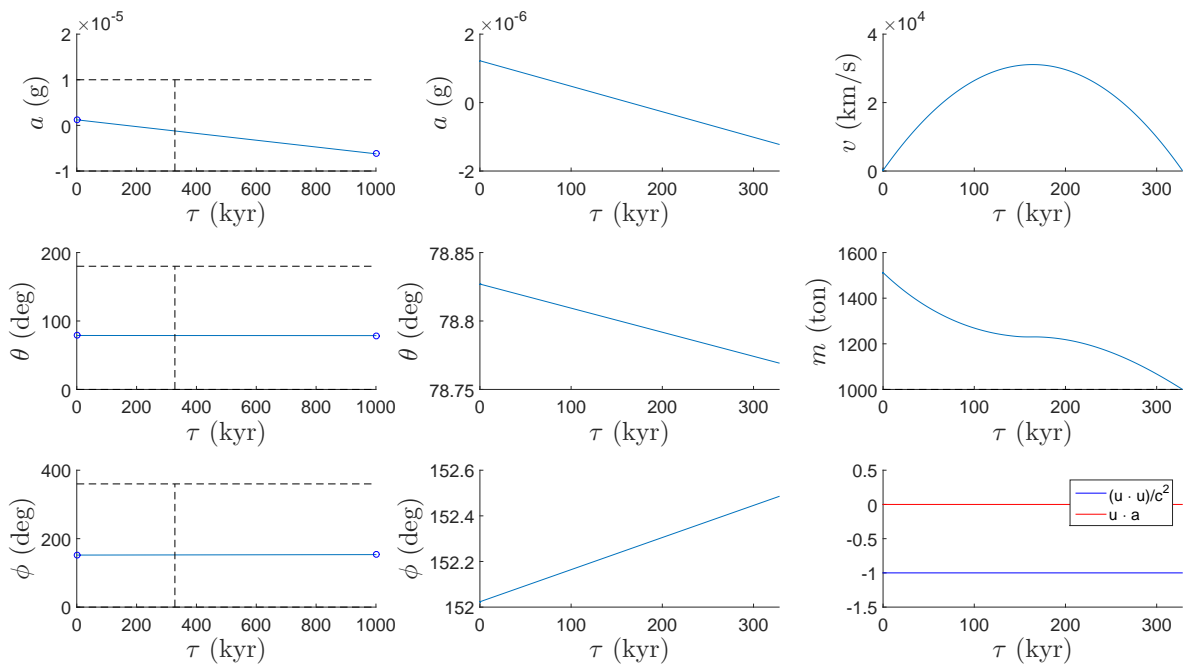Figure 5.6: Side view of optimal trajectory to destination C1.

Figure 5.7: Parameters of the trajectory to destination C1.

and three velocity deviations were calculated to be $0.17\,\mathrm{kpc}$ and $1\,\mathrm{km\,s^{-1}}$ respectively. During this journey, a maximum velocity of $0.17c$ was reached, and required a total proper time of $565\,\mathrm{kyr}$. The fuel-to-empty rocket mass ratio β for each propulsion system is shown in Table 5.6.

Propulsion system	β
Fusion rocket	119609
Antimatter rocket	1.18
Photon rocket	0.48

Table 5.5: Fuel-to-empty rocket mass ratio to destination A2.

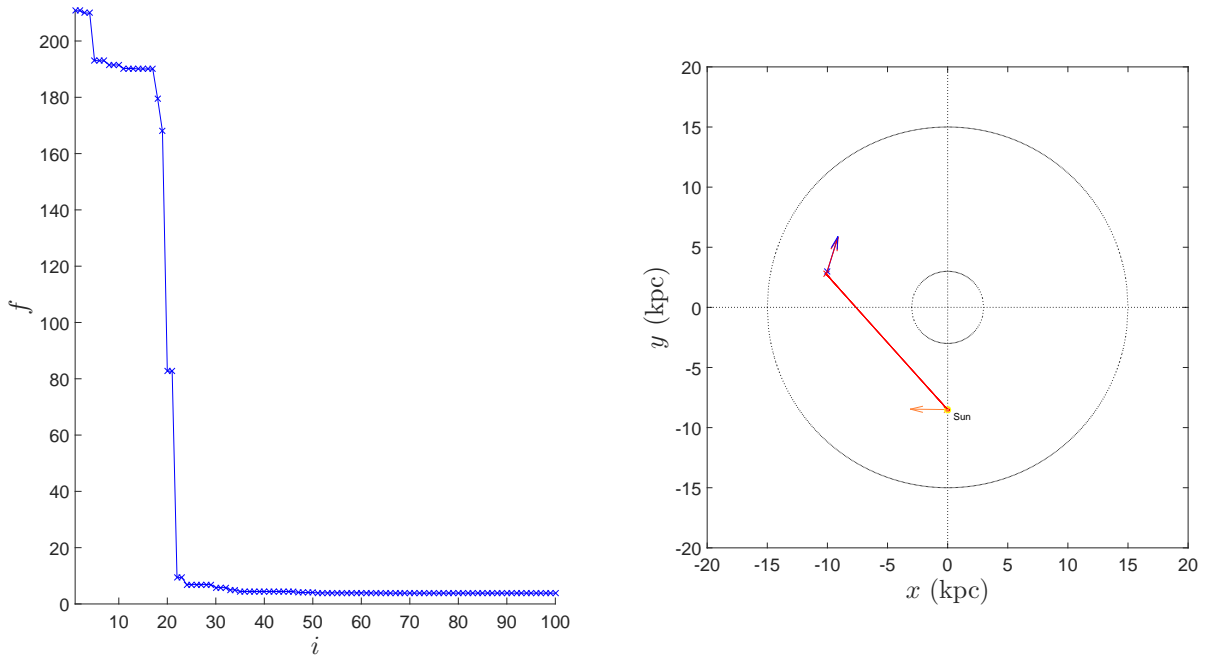Figure 5.8: Fitness (left) and optimal trajectory (right) to destination A2.

Propulsion system	β
Fusion rocket	24034
Antimatter rocket	0.96
Photon rocket	0.40

Table 5.6: Fuel-to-empty rocket mass ratio to destination B2.

5.2.6   Destination C2: The Galactic Halo

The second star system in the galactic halo is located at $(-9, 1, 4)$, about 14 kpc from the Sun. The results are shown in Fig. 5.12 to 5.14. The final position and three velocity deviations were calculated to be 0.27 kpc and 30 km s^{-1} respectively. During this journey, a maximum velocity of 0.10c was reached, and required a total proper time of 643 kyr. The fuel-to-empty rocket mass ratio β for each propulsion system is shown in Table 5.7.
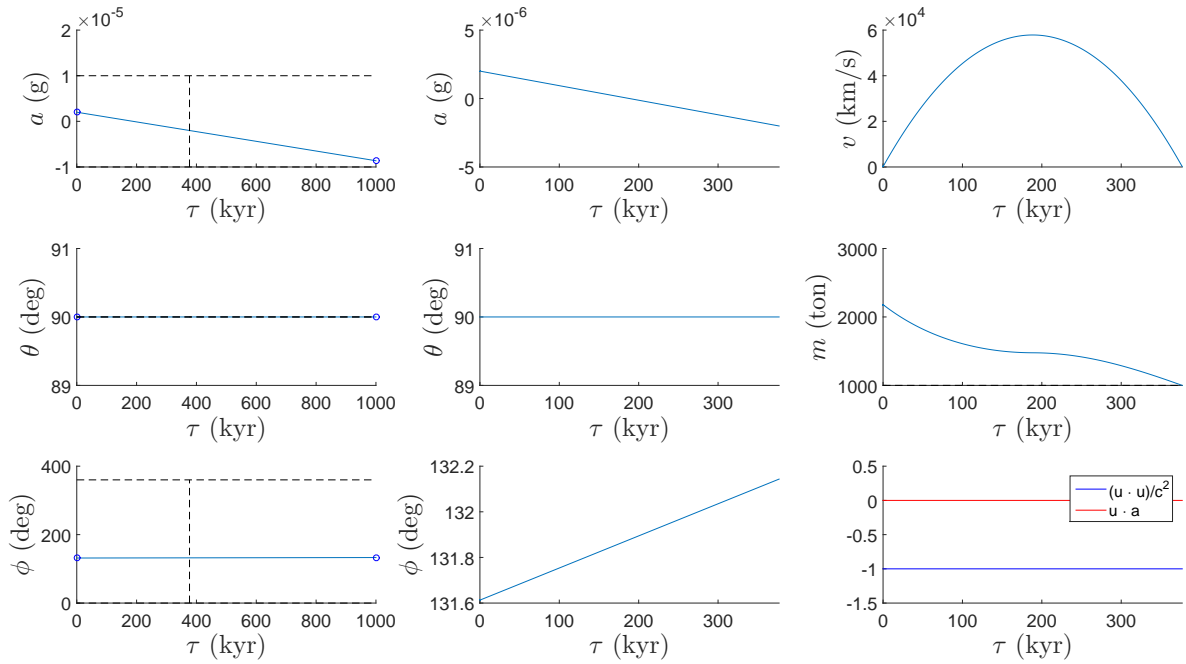
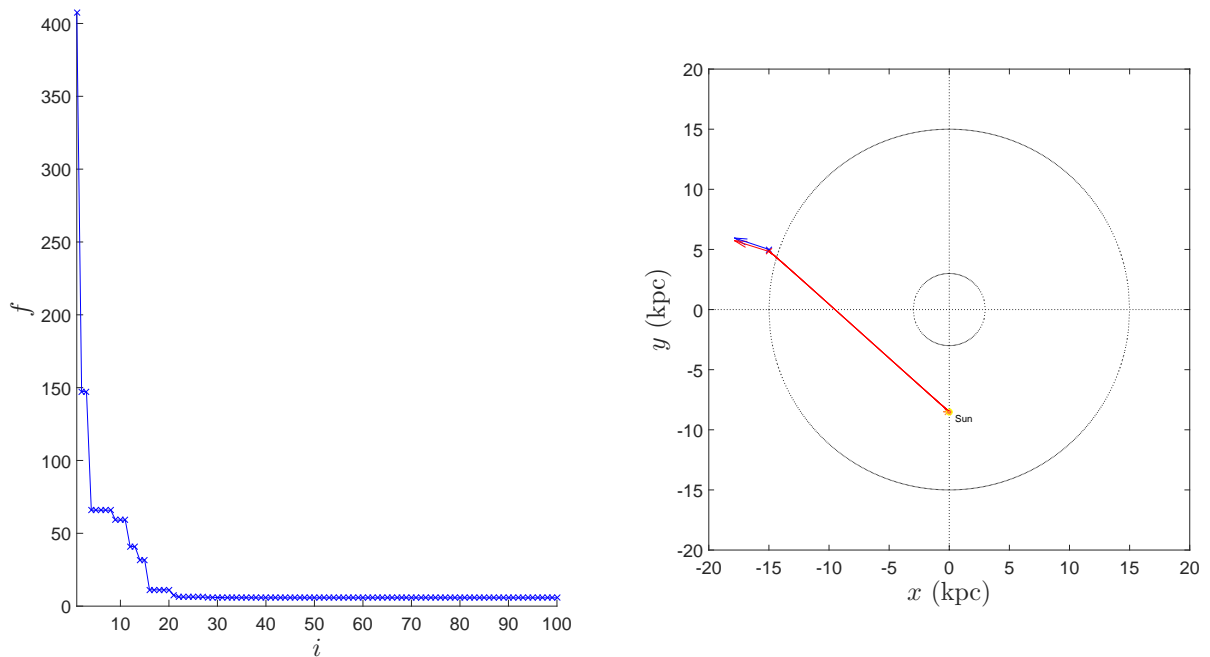Figure 5.9: Parameters of the trajectory to destination A2.

Figure 5.10: Fitness (left) and optimal trajectory (right) to destination B2.

5.2.7 Destination A3: The Galactic Plane

The next star system in the galactic plane is located at $(8, -2, 0)$, about $10\,\text{kpc}$ from the Sun. The results are shown in Fig. 5.15 to Fig. 5.17, where Fig. 5.16 shows a close up of the trajectory at the start and end points. In the right figure, the end point is indicated
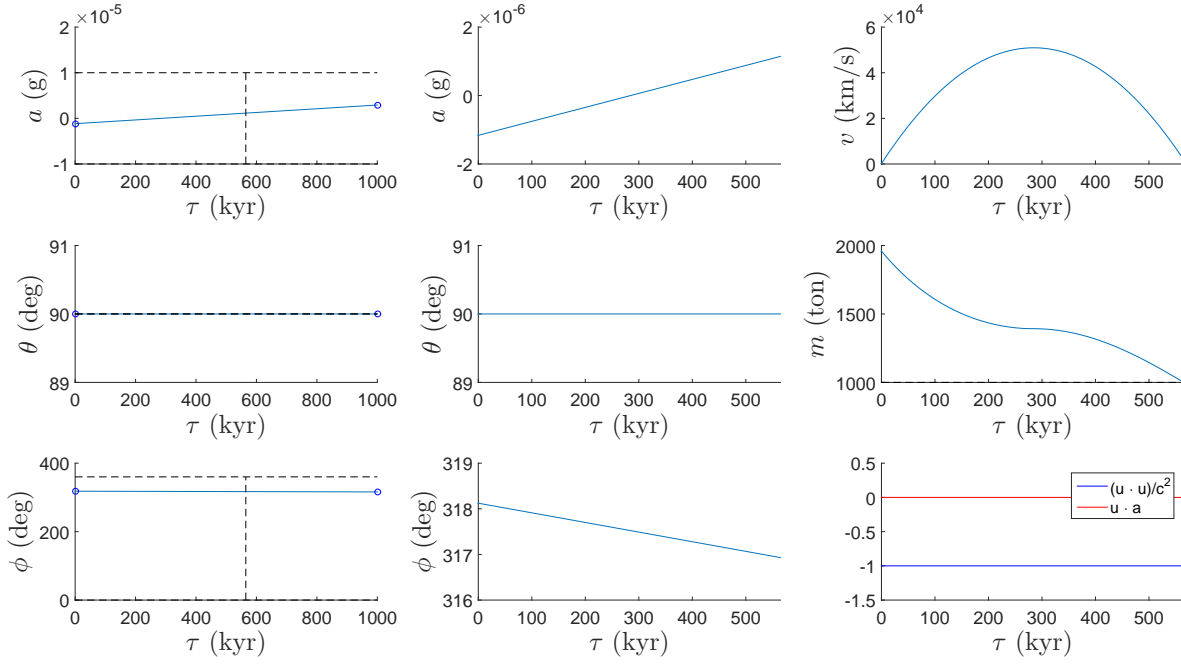
Figure 5.11: Parameters of the trajectory to destination B2.

Propulsion system	β
Fusion rocket	457
Antimatter rocket	0.50
Photon rocket	0.23

Table 5.7: Fuel-to-empty rocket mass ratio to destination C2.

by the red cross, and the straight line shown is a portion of the final velocity vector. The final position and three velocity deviations were calculated to be $0.07\,\mathrm{kpc}$ and $5\,\mathrm{km\,s^{-1}}$ respectively. During this journey, a maximum velocity of $0.15c$ was reached, and required a total proper time of $336\,\mathrm{kyr}$. The fuel-to-empty rocket mass ratio β for each propulsion system is shown in Table 5.8.

Propulsion system	β
Fusion rocket	8074
Antimatter rocket	0.82
Photon rocket	0.35

Table 5.8: Fuel-to-empty rocket mass ratio to destination A3.

5.2.8   Destination B3: A Hypervelocity Star

The final HVS is located at $(12, -1, 0)$, about $14\,\mathrm{kpc}$ from the Sun, and with a velocity magnitude of $2000\,\mathrm{km\,s^{-1}}$. The results are shown in Fig. 5.18 and 5.19. The final position
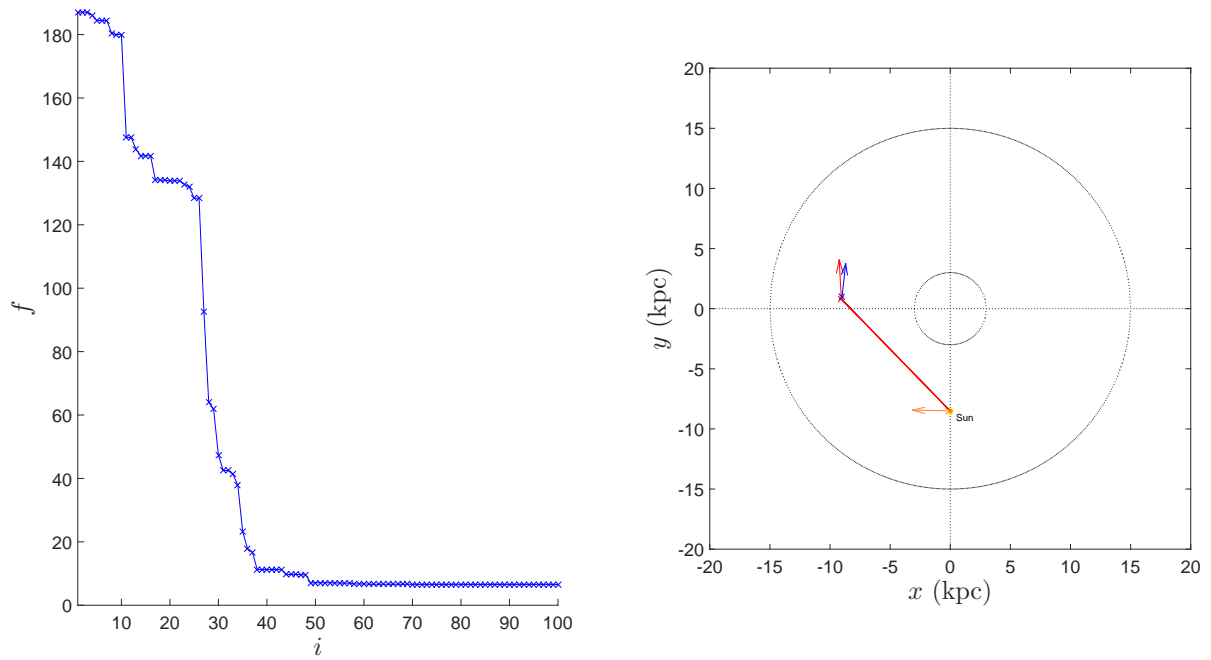
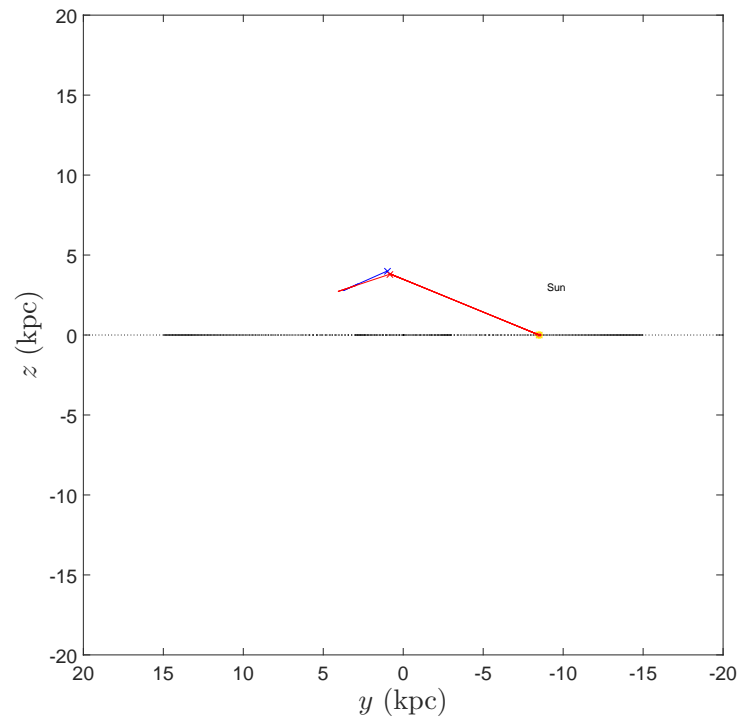Figure 5.12: Fitness (left) and optimal trajectory (right) to destination C2.

Figure 5.13: Side view of optimal trajectory to destination C2.

and three velocity deviations were calculated to be $0.08\,\mathrm{kpc}$ and $21\,\mathrm{km\,s^{-1}}$ respectively. During this journey, a maximum velocity of $0.18c$ was reached, and required a total proper time of 375 kyr. The fuel-to-empty rocket mass ratio β for each propulsion system is shown in Table 5.9.
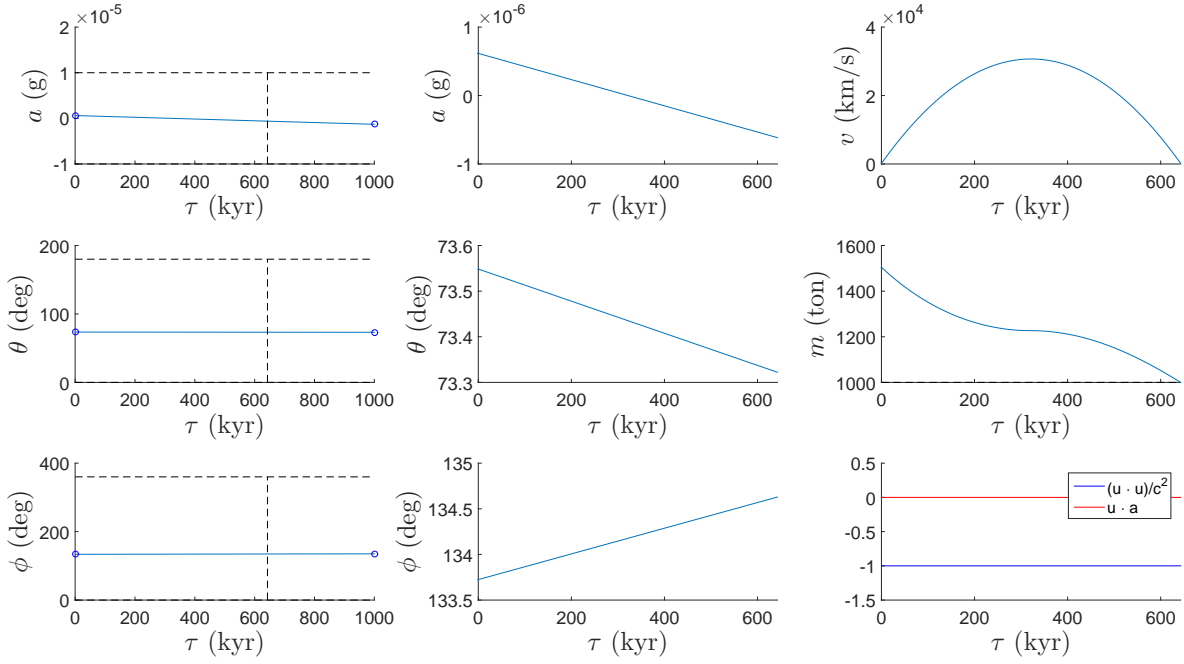
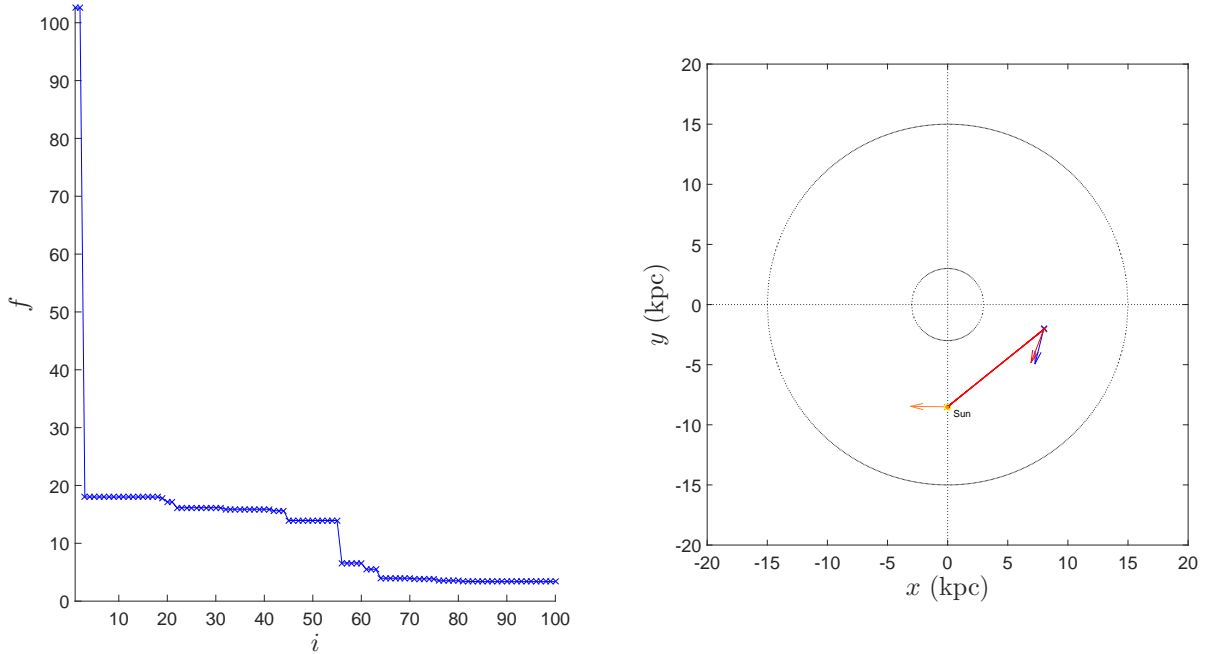Figure 5.14: Parameters of the trajectory to destination C2.

Figure 5.15: Fitness (left) and optimal trajectory (right) to destination A3.

5.2.9   Destination C3: The Galactic Halo

The final star system in the galactic halo is located at $(8, -2, 3)$, about $11\,\text{kpc}$ from the Sun. The results are shown in Fig. 5.20 to 5.22. The final position and three velocity deviations were calculated to be $1.14\,\text{kpc}$ and $22\,\text{km\,s}^{-1}$ respectively. During this journey,
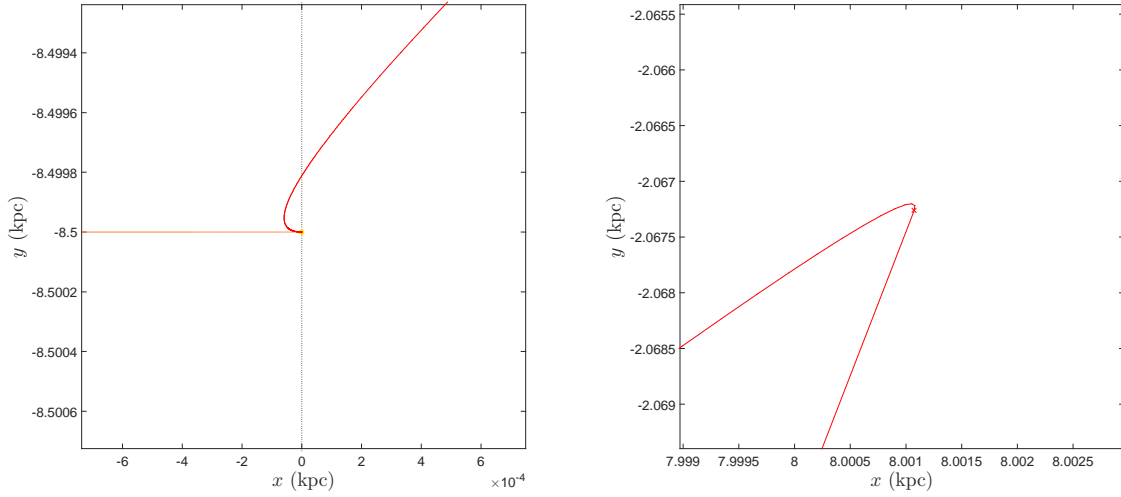
Figure 5.16: Close up view of the optimal trajectory to destination A3 at the start (left) and end (right) points.
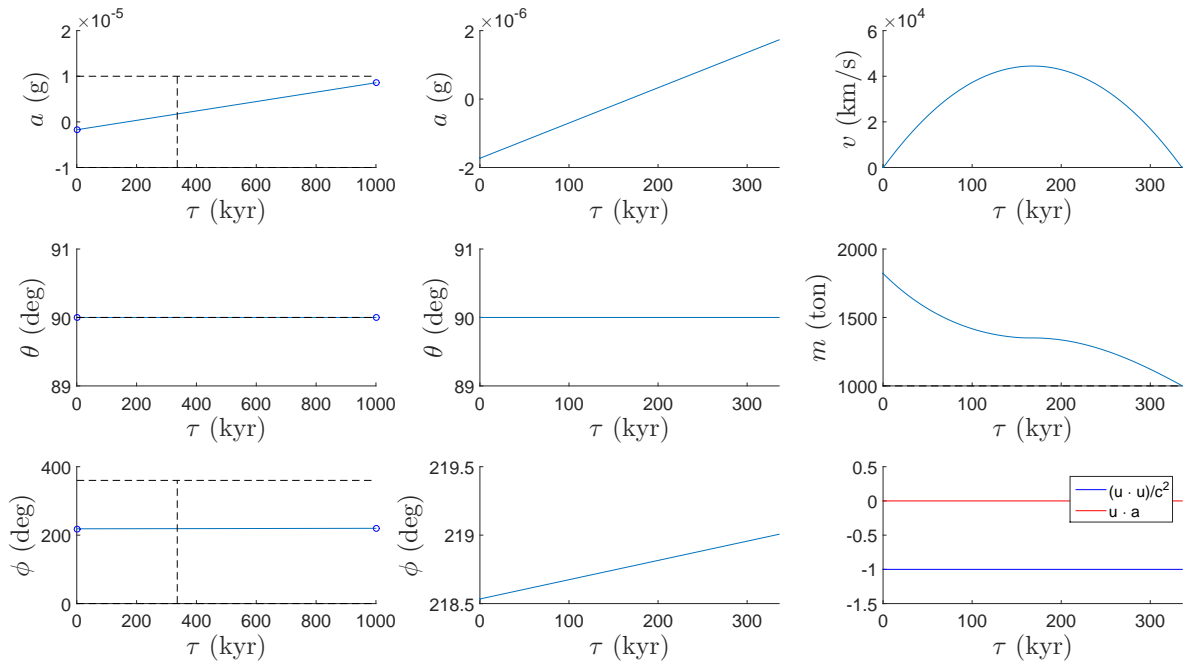
Figure 5.17: Parameters of the trajectory to destination A3.

Propulsion system	β
Fusion rocket	46867
Antimatter rocket	1.05
Photon rocket	0.43

Table 5.9: Fuel-to-empty rocket mass ratio to destination B3.

a maximum velocity of $0.13c$ was reached, and required a total proper time of $397\,\mathrm{kyr}$. The fuel-to-empty rocket mass ratio β for each propulsion system is shown in Table 5.10.
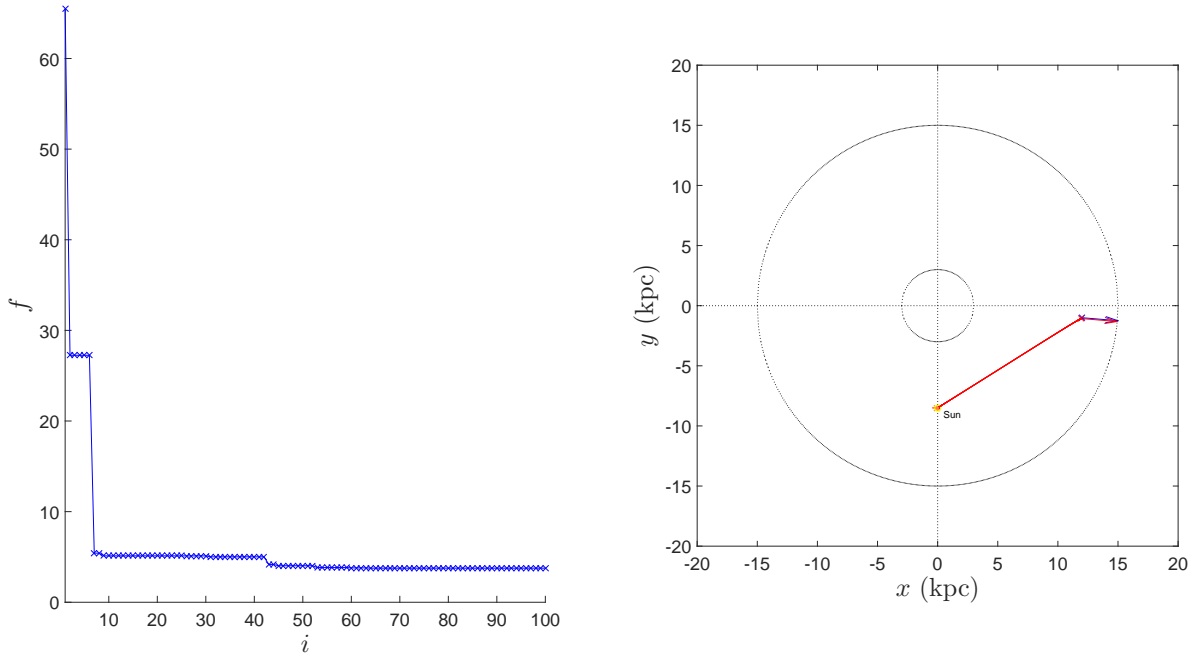
Figure 5.18: Fitness (left) and optimal trajectory (right) to destination B3.
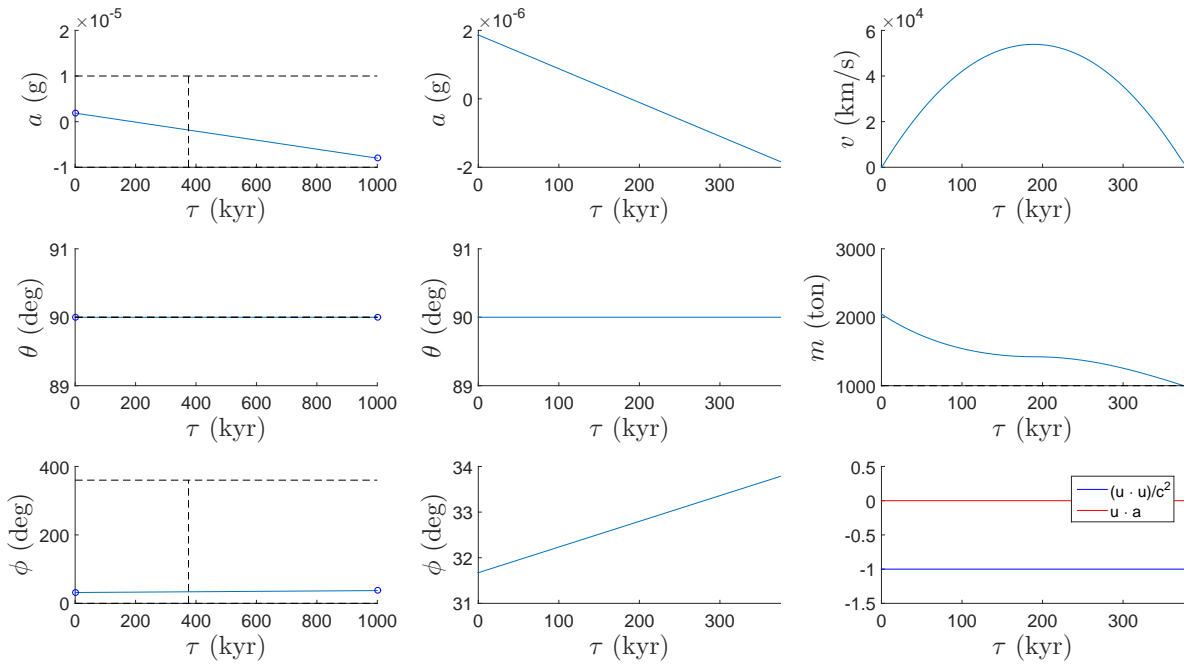
Figure 5.19: Parameters of the trajectory to destination B3.

5.3   Discussion

A summary of the results is shown in Table 5.11. For destinations within the galactic plane, the genetic algorithm is able to calculate optimal trajectories that arrive within $0.25\,\mathrm{kpc}$ and $35\,\mathrm{km\,s^{-1}}$ of the desired star system. However, the algorithm struggles to

Propulsion system	β
Fusion rocket	2048
Antimatter rocket	0.66
Photon rocket	0.29

Table 5.10: Fuel-to-empty rocket mass ratio to destination C3.
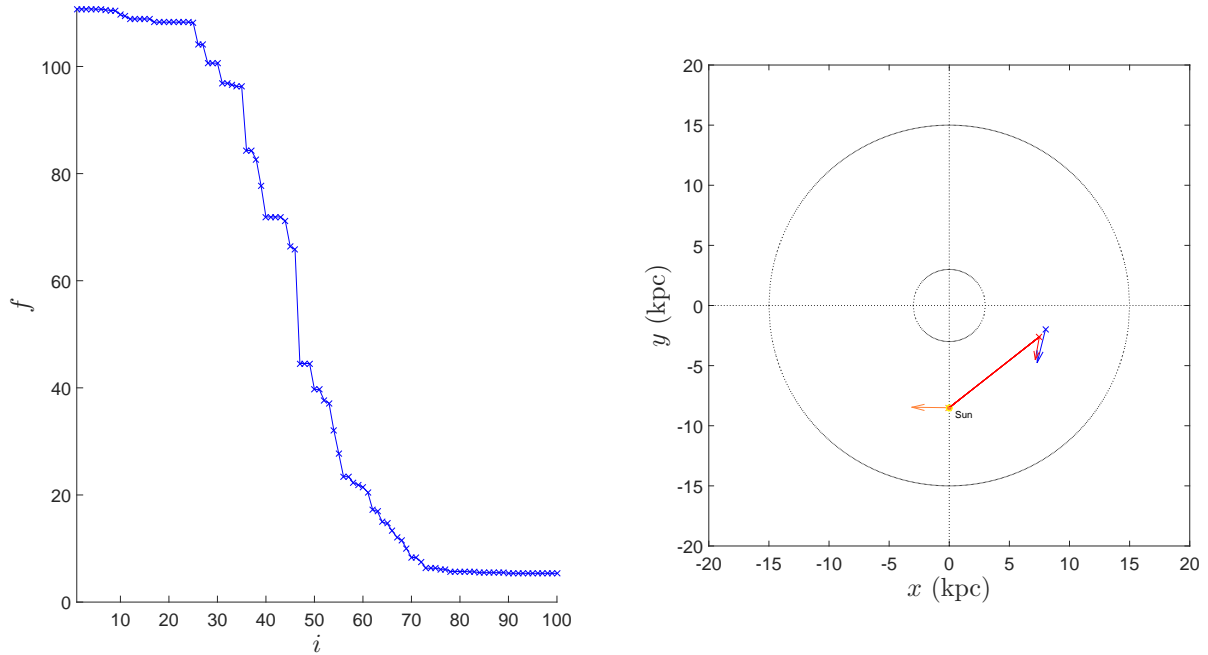
Figure 5.20: Fitness (left) and optimal trajectory (right) to destination C3.

find high quality solutions for destinations outside the galactic plane. A larger sample size and/or a higher number of generations are likely required to generate more accurate solutions to these destinations. The number of binary digits seems to be sufficient in each of the cases considered, and do not need to be increased unless one wishes to further refine a particular solution. For 200 samples and 100 generations, about 60 mins was required for each application of the algorithm using a quad-core, 2.6 GHz CPU with 8 GB of RAM.

| Destination	A1	B1	C1	A2	B2	C2	A3	B3	C3
Distance (kpc)	8	10	7	15	20	14	10	14	11
Distance deviation (kpc)	0.09	0.17	0.73	0.24	0.17	0.27	0.07	0.08	1.14
Velocity deviation ($\mathrm{km\,s^{-1}}$)	23	33	10	12	1	30	5	21	22
Proper time taken (kyr)	351	390	328	377	565	643	336	375	397
Maximum velocity (c)	0.11	0.12	0.10	0.19	0.17	0.10	0.15	0.18	0.13
β_{fusion}	10^3	10^3	10^2	10^5	10^4	10^2	10^4	10^4	10^3
$\beta_{\mathrm{antimatter}}$	0.53	0.62	0.51	1.18	0.96	0.50	0.82	1.05	0.66
β_{photon}	0.24	0.27	0.23	0.48	0.24	0.23	0.35	0.43	0.29

Table 5.11: Summary of results.

Figure 5.21: Side view of optimal trajectory to destination C3.
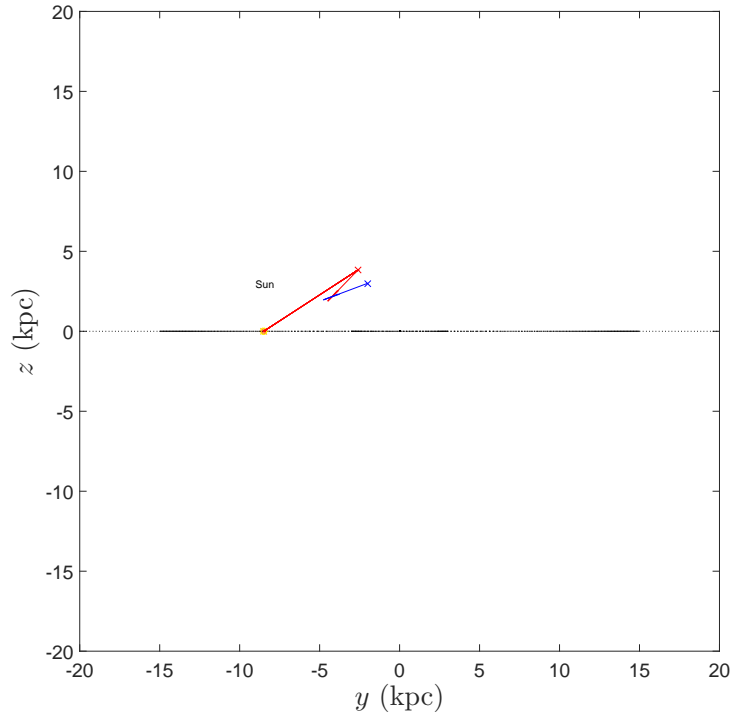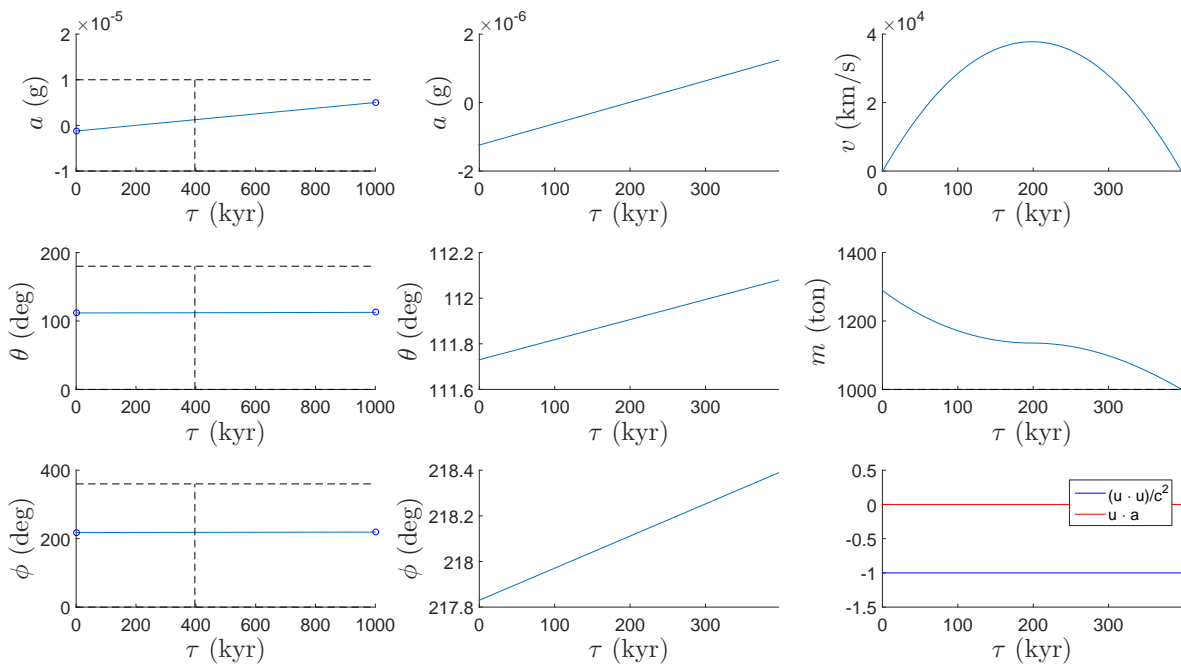

Figure 5.22: Parameters of the trajectory to destination C3.

Inspection of the normalisation values in each of the scenarios shows that the Matlab ODE solver calculated the variables to a high degree of accuracy. The linear acceleration profile also leads to a parabolic velocity profile, which in turn leads to the consistent mass function curves as seen above.

The use of the various propulsion systems clearly has a significant impact on the fuel-to-empty mass ratio β. For a low-acceleration rocket with a linear acceleration profile, the use of a photon drive results in β values below 0.50, with values as low as 0.24. An antimatter drive produces β values between 0.50 and 1.2, though most stay below 1.0. These values are similar to the chemical rockets in use today. The β values of the fusion drive are on the order of 10^2, and reach as high as 10^5. Clearly, a fusion drive would not be practical for such journeys. An antimatter drive would likely be the minimum technological requirement for an interstellar journey. This would apply for even high acceleration journeys, since high accelerations generally require high rates of fuel consumption, which in turn results in a heavier spacecraft. However, high accelerations require shorter travel times, and this trade-off is one that is frequently encountered in trajectory optimisation problems.

Upon inspection of each of the trajectories, it is evident that the gravitational potential has minimal effect on the trajectory of a low-acceleration rocket. In each case, the maximum velocity reached is between $0.1c$ and $0.2c$. While these speeds may appear large, they are still non-relativistic, with corresponding Lorentz factors of 1.005 and 1.021 respectively. At these speeds, roughly 350-400 kyr was required to reach most of the destinations (with the exceptions being Locations B2 and C2). Clearly, this is not very practical for manned interstellar travel. To achieve more practical solutions, the maximum allowable acceleration magnitude would need to be increased. However, doing so raises many issues that would need to be addressed, and these are discussed in the final chapter.

Chapter 6

Conclusion

Problem statement: *How should we vary the thrust and orientation of a low-acceleration rocket such that a traveller reaches a galactic destination in the least possible time? Knowing this, how viable is galactic colonisation using low-acceleration rockets?*

The results of this research have demonstrated the use of genetic algorithms to optimise interstellar trajectories using a low-acceleration rocket. By varying the magnitude and orientation of the acceleration vector, we have calculated optimal paths to several galactic destinations. The algorithm showed remarkable success for destinations within the galactic plane, but produced less successful results for destinations outside the galactic plane. To produce more accurate trajectories to destinations outside the galactic plane, the sample size and/or number of generations would need to be increased.

For the mass calculations, three types of propulsive systems were considered: the fusion drive, antimatter drive, and the photon drive. The fuel-to-empty rocket mass ratio for each of these were calculated, and it was concluded that for a linear acceleration profile, the antimatter drive would represent the minimum technological requirement when undertaking an interstellar journey. The calculated values are conservative since low accelerations generally require low fuel consumption. However, low accelerations require longer travel times; for each interstellar destination, low-acceleration rockets required several hundreds of thousands of years to reach their destination. Clearly, galactic colonisation is highly unrealistic using low-acceleration rockets.

6.1   Future Work

The optimal trajectories calculated in this research have only considered the use of low-acceleration rockets. Future work may involve increasing the acceleration limits to much higher values, say 1 g, which would allow for a comfortable journey. It would then be interesting to assess the possibility of galactic colonisation using a photon drive, and if the answer is still "not very possible", then this would lead us to ask exactly what type of

propulsion system would be required for galactic colonisation.

As mentioned in the beginning chapter, Kwan et al. (2010) showed that a rocketeer accelerating at a constant 1 g can reach the edge of the universe within a human lifetime, meaning that interstellar travel can theoretically be achieved within decades, if not years. However, calculating trajectories with high accelerations over extended periods of time creates many hurdles that need to be addressed from a computational viewpoint.

Firstly, the genetic algorithm needs to find a path that reaches the star system with the correct final velocity. This becomes more difficult if the maximum allowable acceleration magnitude is increased, since small deviations to the acceleration can result in significant changes to the trajectory. Consequently, the binary digits would need to be greatly increased to enhance the resolution of each variable, which in turn requires longer computational times.

Another main problem is due to the limitation of machine precision of Matlab. Large accelerations over extended periods of time will push the velocity closer and closer to the speed of light. Consider a rocket accelerating indefinitely at 1 g along the x-axis in flat spacetime. Near the speed of light, the Lorentz factor approaches infinity, and $u^t \to u^x$. At this stage, the normalisation values will begin to diverge since round-off errors are introduced, which compromises the accuracy of the results. As the velocity keeps increasing, the integration will reach a point when u^t effectively equals u^x due to machine precision. At this point, the normalisation values drop abruptly to zero, and the proper time cannot be accurately computed or verified.

Overcoming these obstacles would require a new approach, likely requiring the reformulation of the equations of motion to prevent the introduction of any infinities. Alternatively, one could attempt to force the spacecraft to slow down once a specified velocity is reached to ensure that the normalisation values are stable. Increasing the number of spline points could help solve this problem, though this would greatly increase the computational time required for each trajectory calculation. However, it would be interesting to see if increasing the spline points drastically affects the fuel-to-empty rocket mass ratio β and the proper time taken. If significant reductions in β or the proper time are achieved, then the increased computational cost could possibly be justified.

Another topic of future work could focus on finding an alternative method to compute the optimal proper time from the linear acceleration profile. In the current framework, the spline points are fitted between 0 and some maximum proper time, and the curve is truncated at a particular point. Consequently, this limits the possible solutions since the two spline points are plotted at the ends. Increasing the number of spline points is one possible solution, but is not ideal due to the computational cost mentioned before.

Whilst a significant amount of research has been conducted so far, there is clearly considerable room for further investigation. Galactic colonisation may indeed one day be possible, but supporting such a claim would require further research into this topic.

"The heavens declare the glory of God;
the skies proclaim the work of his hands."

(Psalm 19:1)

Bibliography

Abdelkhalik, O. and Mortari, D. (2007). N-impulse orbit transfer using genetic algorithms. *Journal of Spacecraft and Rockets*, 44(2):456–460.

Ackeret, J. (1946). Zur theorie der raketen (On the theory of rockets). *Helvetica Physica Acta*, 19(2):103–112.

Bade, W. (1953). Relativistic rocket theory. *American Journal of Physics*, 21(4):310–312.

Baumgardt, H., Gualandris, A., and Zwart, S. P. (2006). Ejection of hypervelocity stars from the Galactic Centre by intermediate-mass black holes. *Monthly Notices of the Royal Astronomical Society*, 372(1):174–182.

Bennett, C., Larson, D., Weiland, J., Jarosik, N., Hinshaw, G., Odegard, N., Smith, K., Hill, R., Gold, B., Halpern, M., et al. (2013). Nine-year Wilkinson Microwave Anisotropy Probe (WMAP) observations: final maps and results. *The Astrophysical Journal Supplement Series*, 208(2):20.

Betts, J. T. (1998). Survey of numerical methods for trajectory optimization. *Journal of guidance, control, and dynamics*, 21(2):193–207.

Bullock, J. S. and Johnston, K. V. (2005). Tracing galaxy formation with stellar halos. I. Methods. *The Astrophysical Journal*, 635(2):931–949.

Cassenti, B. (1997). Optimisation of Interstellar Solar Sail velocities. *Journal of the British Interplanetary Society*, 50(12):475–478.

Charbonneau, P. (1995). Genetic algorithms in astronomy and astrophysics. *The Astrophysical Journal Supplement Series*, 101:309.

Cheng, T.-P. (2015). *A College Course on Relativity and Cosmology*. Oxford University Press, 1st edition.

Coley, D. A. (1999). *An Introduction to Genetic Algorithms for Scientists and Engineers*. World Scientific.

Dachwald, B. (2004). Low-thrust trajectory optimization and interplanetary mission analysis using evolutionary neurocontrol. *Doktorarbeit, Institut für Raumfahrttechnik, Universität der Bundeswehr, München*.

Dachwald, B. (2005). Optimal solar sail trajectories for missions to the outer solar system. *Journal of Guidance, Control, and Dynamics*, 28(6):1187–1193.

Darwin, C. (1859). *On the Origins of Species*. D. Appleton and Company.

de Naray, R. K., McGaugh, S. S., and Mihos, J. C. (2009). Constraining the NFW potential with observations and modeling of low surface brightness galaxy velocity fields. *The Astrophysical Journal*, 692(2):1321.

Dehnen, W., McLaughlin, D. E., and Sachania, J. (2006). The velocity dispersion and mass profile of the Milky Way. *Monthly Notices of the Royal Astronomical Society*, 369(4):1688–1692.

Down East Engineering (2014). *Christoffel symbols and geodesics, symbolic model.* http://au.mathworks.com/matlabcentral/fileexchange/45901-christoffel-symbols-and-geodesics–symbolic-model.

Einstein, A. (1905). Zur elektrodynamik bewegter körper (On the Electrodynamics of Moving Bodies). *Annalen der physik (Annals of Physics)*, 322(10):891–921.

Einstein, A. (1907). Relativittsprinzip und die aus demselben gezogenen Folgerungen (On the Relativity Principle and the Conclusions Drawn from It). *Jahrbuch der Radioaktivitt (Yearbook of Radioactivity)*, 4(411462):454.

Einstein, A. (1915). Die feldgleichungen der gravitation (The field equations of gravitation). *Sitzungsberichte der Königlich Preußischen Akademie der Wissenschaften (Berlin), Seite 844-847 (Proceedings of the Prussian Academy of Sciences (Berlin), Pages 844-847)*, 1:844–847.

Esnault-Pelterie, R. and Lahure, A. (1930). L'Astronautique (Astronautics). *Paris*, 2:114–117.

Feynman, R., Leighton, R., and Sands, M. (2011). *The Feynman Lectures on Physics*, volume 1. Basic Books.

Gasperini, M. (2013). *Theory of Gravitational Interactions*. Springer.

Glendenning, N. K. (2007). *Our Place in the Universe*. World Scientific Publishing Company.

Griffiths, D. (1999). *Introduction to Electrodynamics*. Addison-Wesley, 3rd edition.

Grøn, Ø. and Hervik, S. (2007). *Einstein's General Theory of Relativity: With Modern Applications in Cosmology*. Springer.

Hartle, J. B. (2003). *Gravity: An Introduction to Einstein's General Relativity*, volume 1. Addison-Wesley.

Henriques, P. G. and Natario, J. (2012). The rocket problem in general relativity. *Journal of Optimization Theory and Applications*, 154(2):500–524.

Hernquist, L. (1990). An analytical model for spherical galaxies and bulges. *The Astrophysical Journal*, 356:359–364.

Heyl, J. S. (2005). The long-term future of space travel. *Physical Review D*, 72(10):107302.

Hills, J. G. (1988). Hyper-velocity and tidal stars from binaries disrupted by a massive Galactic black hole. *Nature Publishing Group*.

Jones, M. H. and Lambourne, R. J. (2004). *An Introduction to Galaxies and Cosmology*. Cambridge University Press.

Kafle, P. R., Sharma, S., Lewis, G. F., and Bland-Hawthorn, J. (2012). Kinematics of the Stellar Halo and the Mass Distribution of the Milky Way Using Blue Horizontal Branch Stars. *The Astrophysical Journal*, 761(1210.7527):98.

Kafle, P. R., Sharma, S., Lewis, G. F., and Bland-Hawthorn, J. (2014). On the Shoulders of Giants: Properties of the Stellar Halo and the Milky Way Mass Distribution. *The Astrophysical Journal*, 794(1):59.

Kerr, F. J. and Lynden-Bell, D. (1986). Review of galactic constants. *Monthly Notices of the Royal Astronomical Society*, 221(4):1023–1038.

Kluever, C. A. (1996). Trajectory Optimization of an Interstellar Mission Using Solar Electric Propulsion. *NASA*, (19980004505).

Koposov, S. E., Rix, H. W., and Hogg, D. W. (2010). Constraining the Milky Way Potential with a Six-Dimensional Phase-Space Map of the GD-1 Stellar Stream. *The Astrophysical Journal*, 712:260–273.

Koupelis, T. and Kuhn, K. F. (2007). *In Quest of the Universe*. Jones & Bartlett Learning, 5th edition.

Kwan, J., Lewis, G. F., and James, J. B. (2010). The Adventures of the Rocketeer: Accelerated Motion Under the Influence of Expanding Space. *Publications of the Astronomical Society of Australia*, 27(1):15–22.

Matloff, G. L. (2010). *Deep Space Probes: To the Outer Solar System and Beyond*. Springer, 2nd edition.

Miyamoto, M. and Nagai, R. (1975). Three-dimensional models for the distribution of mass in galaxies. *Publications of the Astronomical Society of Japan*, 27:533–543.

Moore, P. and Rees, R. (2011). *Patrick Moore's Data Book of Astronomy*. Cambridge University Press, 2nd edition.

Moore, W. (1813). A treatise on the motion of rockets. *London: G. and S. Robinson*, page 13.

Morin, D. (2008). *Introduction to Classical Mechanics: With Problems and Solutions*. Cambridge University Press, 1st edition.

Navarro, J. F., Frenk, C. S., and White, S. D. (1997). A Universal density profile from hierarchical clustering. *The Astrophysical Journal*, 490(2):493.

Newton, I. (1687). *Philosophiæ Naturalis Principia Mathematica*. Edmund Halley.

Nusser, A. (2009). Ergodic Considerations in the Gravitational Potential of the Milky Way. *The Astrophysical Journal*, 706(1):113–118.

Powell, J. R. and Pelligrino, C. (1987). A matter-antimatter propulsion system for manned interstellar flight. Number BNL-40082. Brookhaven National Lab., Upton, NY (USA).

Rindler, W. (1960). Hyperbolic motion in curved space time. *Physical Review*, 119(6):2082–2089.

Rix, H.-W. and Bovy, J. (2013). The Milky Way's stellar disk. *The Astronomy and Astrophysics Review*, 21(1):1–58.

Seeds, M. A. and Backman, D. (2015). *Stars and Galaxies*. Cengage Learning, 9th edition.

Stephani, H. (2004). *Relativity: An Introduction to Special and General Relativity*. Cambridge University Press, 3rd edition.

Tinder, R. F. (2006). *Relativistic Flight Mechanics and Space Travel: A Primer for Students, Engineers and Scientists (Synthesis Lectures on Engineering Series)*. Morgan and Claypool Publishers.

Tsiolkovsky, K. (1903). The exploration of cosmic space by means of reaction devices. *Scientific Review*, (5).

Vinkó, T. and Izzo, D. (2008). Global optimisation heuristics and test problems for preliminary spacecraft trajectory design. *European Space Agency, The Advanced Concepts Team*.

Zeng, X., Li, J., Baoyin, H., and Gong, S. (2011). Trajectory optimization and applications using high performance solar sails. *Theoretical and Applied Mechanics Letters*, 1(3):033001.